



**Universitatea  
BABEȘ-BOLYAI**



**BABEȘ-BOLYAI UNIVERSITY CLUJ-NAPOCA  
FACULTY OF PHYSICS**

**Structural studies for some compounds with biological  
activity**

**PhD Thesis Summary**

**PhD student  
Turza Ioan Alexandru**

**PhD supervisor  
PROF. DR. Pop Aurel**

**CLUJ-NAPOCA  
2021**





**Universitatea  
BABEȘ-BOLYAI**



**BABEȘ-BOLYAI UNIVERSITY CLUJ-NAPOCA  
FACULTY OF PHYSICS**

**Structural studies for some compounds with biological  
activity**

**PhD student  
Turza Ioan Alexandru**

**PhD supervisor  
PROF. DR. Pop Aurel**

**CLUJ-NAPOCA  
2021**

**KEY WORDS:** Biologically active compounds: diuretics, steroids, SARMs, Cu complexes with sulfonamides; Crystallization and solid forms; X-ray single crystal and powder diffraction; Spectroscopic and thermal analysis (IR, Raman, DSC, TG); lattice energy; intermolecular interactions

## Table of contents

<b>Introduction</b>	<b>8</b>
<b>1. Structural characterization methods of pharmaceutical compounds and their solid forms</b>	<b>9</b>
1.1. Methods of single crystals growth and obtaining new solid forms	9
1.2. Symmetry in crystals	11
1.3. Generation and monochromatization of X-rays	12
1.4. X-rays diffraction	13
1.5. Crystal structure determination from single crystals diffraction	16
1.6. Crystal structure determination from powder diffraction	18
1.7. Spectroscopic and thermal methods	19
1.8. Intermolecular interactions and lattice energy by CLP and Hirshfeld surfaces	20
1.9. Conformational analysis for five and six membered rings	21
<b>2. Structural characterization of steroid compounds</b>	<b>23</b>
2.1. Anabolic-androgenic steroids, an overview	23
<b>2.2. Boldenone and boldenone esters</b>	<b>24</b>
2.2.1. General features of boldenone	24
2.2.2. Crystallization experiments and X-ray diffraction analysis	25
2.2.3. Crystal structures determination and analysis	25
2.2.4. Hirshfeld surfaces, fingerprint plots and evaluation of lattice energies	32
2.2.5. Conformational rings analysis of boldenone based compounds	38
2.2.6. Conclusions for boldenone-based compounds	39
<b>2.3. Trenbolone and trenbolone esters</b>	<b>39</b>
2.3.1. Overview and features for trenbolone	39
2.3.2. Crystallization experiments and X-ray diffraction analysis	41
2.3.3. Crystal structures determination and analysis	42
2.3.4. Hirshfeld surfaces, fingerprint diagrams and lattice energies evaluation	47
2.3.5. Conformational rings analysis of trenbolone based compounds	53
2.3.6. Conclusions for trenbolone-based compounds	54
<b>2.4. Drostanolone propionate and its polymorphs</b>	<b>55</b>
2.4.1. Overview and particularities of drostanolone	55
2.4.2. Crystallization experiments and X-ray diffraction analysis	55
2.4.3. Determination of crystal structures and analysis	56
2.4.4. Hirshfeld surfaces, fingerprint plots and lattice energies evaluation	60
2.4.5. Conformational rings analysis of drostanolone propionate polymorphs	67
2.4.6. Conclusions for drostanolone propionate polymorphism	68

<b>3. Structural analysis of ostarine and andarine. Selective androgen receptor modulators compounds (SARMs)</b>	<b>69</b>
3.1. Biological studies and use of ostarine and andarine	69
3.2. Experimental methods of investigation	70
3.2. Thermal and spectroscopic analysis	71
3.3. Crystal structure determination and analysis of ostarine and andarine	73
3.4. Ostarine polymorph obtaining by phase transformation and crystal structure determination from powders	77
3.5. Intermolecular interactions Hirshfeld surfaces and lattice energies analysis	79
3.6. Conclusions regarding the analysis of ostarine and andarine	82
<b>4. Structural, spectroscopic and theoretical studies of sodium (2-carbamoylphenoxy) acetate salt</b>	<b>82</b>
4.1. Experimental features and computational details on structural studies of algamon	82
4.2. Crystal structure solve and structural characterization	83
4.3. Highlighting intermolecular interactions through Hirshfeld surfaces	87
4.4. Influence of acidic media on sodium (2-carbamoylphenoxy) acetate salt	92
4.5. Conclusions on the structural features of algamon	93
<b>5. Solid forms of the 4-chloric salicylic acid-5-sulfonamide diuretic compound</b>	<b>93</b>
5.1. Importance of solid forms with respect to the compound under investigation	93
5.2. Experiments for obtaining solid forms and their crystallization	95
5.3. Experimental methods of structural analysis for solid forms obtained	95
5.4. Crystal structures descriptions	96
5.5. Lattice energies analysis for the new solid forms	107
5.6. Analysis of IR spectra for the solid forms obtained	107
5.7. DSC thermal analysis and Hirshfeld surface analysis for polymorphs	111
5.8. Conclusions regarding the structural analysis of solid forms	116
<b>6. Copper complexes with sulfonamides</b>	<b>116</b>
6.1. Generalities regarding the studied complexes	116
6.2.1. L1 ligand (C <sub>16</sub> H <sub>15</sub> N <sub>3</sub> O <sub>2</sub> S <sub>2</sub> ) and C1 complex (C <sub>42</sub> H <sub>40</sub> N <sub>8</sub> O <sub>5</sub> S <sub>4</sub> Cu)	118
6.2.2. Structural analysis of complexes C2 (C <sub>42</sub> H <sub>38</sub> CuN <sub>8</sub> S <sub>4</sub> O <sub>6</sub> ) and 121 C3 (C <sub>40</sub> H <sub>35</sub> CuN <sub>8</sub> S <sub>4</sub> O <sub>5</sub> )	121
6.2.3. Structural analysis of complexes C4 (C <sub>48</sub> H <sub>38</sub> CuN <sub>8</sub> S <sub>4</sub> O <sub>6</sub> ) and C5 (C <sub>43</sub> H <sub>30</sub> CuN <sub>7</sub> O <sub>3</sub> S <sub>2</sub> <sup>+</sup> , C <sub>19</sub> H <sub>14</sub> N <sub>3</sub> O <sub>3</sub> S <sub>2</sub> <sup>-</sup> , 1.25(CH <sub>4</sub> O)	123
6.2.4. Structural analysis of complex C6 (C <sub>68</sub> H <sub>72</sub> CuN <sub>14</sub> S <sub>8</sub> O <sub>8</sub> )	126
6.2.5. Conclusions regarding the studied Cu complexes	127
<b>References</b>	<b>128</b>
<b>List of publications in ISI journals</b>	<b>134</b>

## Introduction

There is a relationship between the structure and properties of pharmaceutical compounds, in the sense that the structure of pharmaceutical compounds greatly influences their physico-chemical properties and them in turn influence the pharmacological characteristics and efficiency in the treatment of various diseases. As an example we can mention the polymorphism of pharmaceutical compounds which is characterized by the fact that polymorphs have the same chemical formula but different packaging, as well as intermolecular interactions, which gives them different solubility and also bioavailability. Also to improve solubility and bioavailability, solid forms are used. In the solid forms we have besides polymorphs, hydrates that contain in the crystalline structure besides the basic compound and water, solvates that incorporate in the crystalline structure the solvent in which it was recrystallized, salts and cocrystals. The difference between salts and cocrystals is that cocrystals are formed on the basis of hydrogen bonds between the base compound and the added cofomer, while in the case of salts there is a complete transfer of protons from the more acidic molecule to the molecule with a more basic character.

Both experimental and computational methods were used for the structural characterization of the investigated compounds. For structural studies of pharmaceutical compounds it is desirable to be as single crystals, because for single crystals compounds the most structural information can be obtained. Therefore, in the investigation is indicated be obtain single crystals by recrystallization. Also at this stage, if various conformers and solvents are added, different solid forms as single crystals or crystalline powders can be obtained. If single crystals have been obtained, then the crystal structure is determined by X-ray single crystal diffraction technique. Otherwise it is tried to determine the crystal structure from powders that involves the following steps: determination of the unit cell (crystallographic system, lattice constants) by indexing the diffraction pattern, establishing the space group by Pawley method, searching for the structural model that can be done by Monte Carlo methods, optimization of the structural model by Rietveld refining. As a highlight of the fact that the crystal structure has been correctly solved, some fit parameters that are specific for single crystals and powders are used. Thus, in the case of single crystals, the parameters  $R_w$  and  $R_1$  are used, which show the match between the calculated diffraction intensities and the experimental ones. In the solving process of crystal structure from powders, the fit parameters are  $R_{wp}$  and  $R_p$ , which show the match between the calculated and the experimental pattern. The smaller the fit parameters, the more reliable the determined crystal structure is. It is generally intended that the fit parameters to reach the value of at least 0.1 (10%).

Other useful information in the characterization of pharmaceutical compounds are obtained by thermal methods: DSC, DTA, TG. DSC or DTA can highlight phase transformations and their endo or exothermic nature, the presence of solvents in crystalline structures, melting points and degradation of samples. TG completes the

information obtained through DSC and DTA in the sense that are obtained quantitative characteristics regarding the mass variation by heating.

IR and Raman spectroscopy provide details about the functional groups and hydrogen bonds within the crystal structure and also highlight the formation of new solid forms.

A more complete characterization of the compounds also implies their energetic investigation. Thus, using the CLP method, the lattice energy was calculated, which gives indications of its stability. The lattice energy calculated by CLP, which is a semi-empirical method, was compared with the DFT method, which is an ab-initio method and it was found that the concordance between the two methods is satisfactory.

Also, the analysis of Hirshfeld surfaces highlighted the intermolecular interactions and their nature. For compounds that have five and six rings specific to steroids in their structure, their conformational analysis was performed.

The thesis approaches various compounds from the following classes: compounds from the steroids group, compounds from the class of selective androgen receptor modulators (SARMs), diuretics, analgesics and copper complexes that have potential in the treatment of cancer.

## **1. Experimental and computational methods applied in the characterization of compounds**

### **Diffraction, spectroscopic and thermal methods**

In this thesis were obtained a large number of single crystals for starting compounds and their solid forms (polymorphs, solvates, hydrates, co-crystals). These were achieved by different crystallization methods: evaporation from solvents or solvent mixtures, slow cooling, grinding followed by recrystallization in solution and parallel crystallization. During the parallel crystallization, the CRISSY/Zinsser Analytic crystallization platform was used, which allows the simultaneous crystallization of a number of 24 samples in various solvents or mixtures of solvents with controlled temperature programs.

### **Diffraction methods**

The acquisition of single crystal X-ray diffraction data was performed at room temperature (293 K) for most crystals but also at low temperature for some single crystals (100 K) using a SuperNova diffractometer, with the tube operating at 50 kV and 0.8 mA, equipped with dual micro sources (Cu and Mo) and Eos CCD detector. Data collection was performed using in most cases Cu K $\alpha$  radiation (1.54184 Å) but also Mo K $\alpha$  radiation (0.71073 Å) for some single crystals. The strategy of data collection, absorption correction, Lorentz, polarization, space group determination were applied in CrysAlis PRO [1]. The crystal structures were solved with the Olex software package [2] using one or more of the following programs embedded in Olex2: SHELXS [3], SHELXD [4] and SHELXT [5] which are based on direct methods and olex2.solve [6] which has the

Charge Flipping procedure implemented. For particular cases, the method of determining the crystal structure for twin crystals was used. All crystal structures were refined with the SHELXL refining program [7] using the least squares minimization technique.

In the refining process, H atoms connected to C atoms were treated by the riding method and placed in idealized positions as follows: CH=0.97 Å for H atoms in CH<sub>2</sub> groups, methyl groups CH<sub>3</sub> [CH=0.96 Å], CH=0.93 Å for aromatic H atoms. Hydrogen atoms bound to nitrogen and oxygen atoms were located by Fourier maps and refined with a constrained distance as follows: N-H=0.85 Å for secondary amide groups (NH<sub>2</sub>) and O-H=0.82 Å for OH groups. For all crystal structures Uiso (H)=1.2Ueq(C, N) was considered for the CH, CH<sub>2</sub> and NH<sub>2</sub> groups and 1.5Ueq (O) for all OH groups.

The crystalline powders patterns were recorded with a Bruker D8 Advance diffractometer, the X-ray tube operating at 40 kV and 40 mA. The diffractometer is equipped with a LINXEYE detector and a germanium monochromator (1 1 1), being used to obtain only CuKα1 radiation. The scan was performed with a step less than 0.01°, generally in the 2θ=3-40° range using the DIFFRAC plus XRD Commander program. This scanning interval is sufficient due to the fact that we have organic compounds with a relatively large unit cell compared to inorganic compounds. X-ray diffraction on powders was used to highlight the purity of the samples and the fact that the single crystals investigated are representative of the samples from which they came. In this sense, the experimental powder diffraction patterns were compared with the simulated ones from the crystal structures obtained from single crystals. Also, if single crystals could not be obtained, the crystal structures were solved from powders.

To obtain the crystal structure from a powder pattern, a multi-step procedure involving the following steps was used: diffraction pattern indexing, Pawley refinement for space group assignment, structural model search, and Rietveld refinement [8].

The pattern indexing were performed in the Reflex module, implemented by BIOVIA as the Materials Studio program [9] with the following distinct methods to have a higher confidence: TREOR90 [10], DICVOL96 [11], X-Cell [12]. Common solutions of the unit cell are usually chosen, which have a high value for figure of merit and all diffraction lines are indexed.

The next stage was the Pawley refinement which confirms the spatial group, the crystallographic system and correlated with the calculated density is assigned the number of molecules in the asymmetric unit.

The search for structural models was done by the optimization method with simulated annealing and parallel tempering. These methods use Monte Carlo procedures and the programs used were Fox [13] and Powder Solve [14] implemented in Materials Studio. The method involves molecular translations, rotations and changes in torsion angles until the experimental powder diffraction matches the simulated one as well as possible, and the difference between the simulated and experimental pattern reaches an

overall minimum. Based on the model obtained, Rietveld is refined using the Reflex module.

The profiles of the diffraction lines are approximated with different functions, the most used being Pseudo-Voight. The full width at half maximum is refined with the parameters U, V, W described by Caglioti's equation [15]. The profile parameters NA and NB were taken into account in the Bragg-Brentano instrumental geometry. Other parameters that are refined are the zero point and the shift of the sample, the parameters of asymmetry of the lines that were made taking into account the Berar-Baldinozzi correction with parameters P1, P2, P3, and P4. A polynomial function of 20 order or greater was used to approximate the diffraction background and the preferential orientation parameters  $a^*$ ,  $b^*$ ,  $c^*$  and R0 were taken into account in a March-Dollase correction. The concordance between the calculated and the experimental diffraction pattern is characterized by the factors Rwp and Rp.

### **Spectroscopic and thermal methods**

FT-IR spectra were obtained using a JTCO 6100 or 6200 FTIR type spectrometers in the 4000 to 400  $\text{cm}^{-1}$  spectral range, with a resolution of 4  $\text{cm}^{-1}$  using the KBr pellet technique. The samples were dispersed in anhydrous KBr and the resulting powder was ground in an agate mortar. The pellet was obtained by pressing the ground mixture into an evacuated mold. The spectra were collected and analyzed with Jasco Spectra Manager v.2 software.

The Raman spectra were recorded with a Raman JASCO NRS 3300 spectrometer, equipped with a CCD detector ( $-69^\circ\text{C}$ ), a 600/mm diffraction grating and an Olympus 100x lens. The 785 nm laser line was used as a source of excitation, its power being set at 137.6 mW. The resulting Raman spectra is an addition of three acquisitions of 120 s each. It was recorded with a resolution of 6.45  $\text{cm}^{-1}$ .

DSC curves were recorded with a DSC-60 Shimadzu differential scanning calorimeter in standard crimped aluminum pans as sample holders and alumina as reference sample. Samples were analyzed in the temperature range 293-650 K under dry nitrogen flow (3.5 L/h) with a heating rate of 10  $\text{K min}^{-1}$ . Shimadzu TA-WS60 and TA60 2.1 software were used to collect and analyze the data. The DSC calorimeter was calibrated with reference standards for zinc and indium.

DTA/TGA measurements were performed with a Shimadzu DTG-60H simultaneous thermogravimetric and differential analyzer. The samples were heated in the range of 24-500  $^\circ\text{C}$  with a heating rate of 10  $^\circ\text{C/min}$ , using an alumina sample cell (diameter 5.8 $\times$ 2.5 mm $^2$ ) under dry nitrogen purge (70 ml/min).

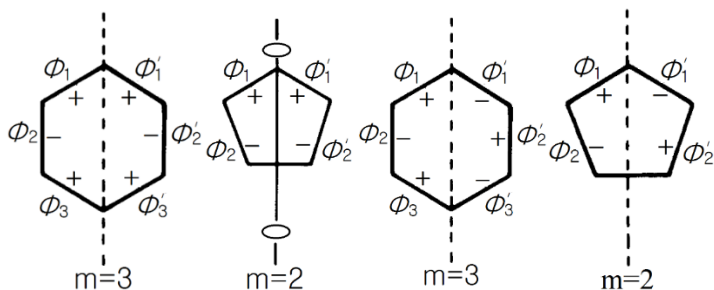
## Investigation of intermolecular contacts and lattice energies

Due to the fact that each compound or solid form has a unique molecular neighborhood, it will interact through intermolecular forces specific to each crystal structure [16]. Highlighting intermolecular interactions can be achieved through Hirshfeld surfaces and corresponding fingerprint diagrams [17,18]. A Hirshfeld molecular surface can be understood on the basis of the blue, white, red color code. The blue zones represent the regions of the crystal where the intermolecular distances are greater than the sum of the van der Waals radii, the white areas have the distances approximately equal to the sum of the van der Waals radii and the strong interactions having the distances shorter than the sum of the van der Waals radii are represented in red. Each Hirshfeld surface can be represented by a two-dimensional diagram on the x-axis being represented the distance from the Hirshfeld surface to the nucleus of an atom inside the surface ( $d_i$ ) and on the y-axis is represented the distance from an atom outside the surface to the Hirshfeld surface ( $d_e$ ) [19]. The points on the fingerprint graph that will have the pairs  $d_i$  and  $d_e$  the smallest, will characterize the atoms involved in the strongest interactions.

The stability of a crystal lattice can be assessed using the lattice energy calculation in the Coulomb-London-Pauli atom-atom approximation developed by Gavezzotti and implemented in the CLP program [20]. In this approximation, the lattice energy is composed of four terms, namely: Coulomb type energy, polarization, dispersion and repulsion. A low lattice energy implies a high stability for the compound, which can also be highlighted by thermal methods relative to melting points or phase transitions. Both Hirshfeld and CLP calculations are performed based on the positions of the atoms in the elementary cell that were previously determined by X-ray diffraction and stored in a CIF file.

## Conformational analysis of five and six membered rings

Because in the thesis there are compounds that have carbon rings of five and six members, it is useful to characterize them in terms of conformational geometry.



$$\Delta C_2 = \sqrt{\frac{\sum_{i=1}^m (\phi_i - \phi_{i'})^2}{m}} \quad \Delta C_s = \sqrt{\frac{\sum_{i=1}^m (\phi_i + \phi_{i'})^2}{m}}$$

The schematic representation of rings with six and five members is given in the figure above. These rings can have a twofold axis or plane of symmetry. It possesses axis of order 2 if the torsion angles are alternately (+, +) and (-, -) and plane of symmetry (mirror plane) if the torsion angles have alternating opposite (+, -). Depending on the existence of the 2nd order axis or the plane of symmetry,  $\Delta C_s$  and  $\Delta C_2$  are defined [21]. If we have ideal symmetry,  $\Delta C_s$  and  $\Delta C_2$  are zero, the higher the value of these parameters, the more deformed the structures will be. The most common structures have the following conformations: chair, half chair, envelope, boat.

## 2. Structural characterization of some steroid compounds

Anabolic-androgenic steroids are a class of compounds, synthetic or naturally occurring that binds to androgen receptors [22], increasing protein synthesis in skeletal muscle and bone tissue. Although anabolic-androgenic steroids possess certain physiological functions that are absolutely necessary in vertebrates and are useful in sports, their abuse and use in the medium and long term can lead to side effects, the most serious being heart related diseases such as ventricular hypertrophy, hypertension, polycythemia, thrombosis [23].

Steroids are often esterified in order to extend the duration of action of the hormone by injection [24].

To improve the properties of steroids, their ability to form polymorphs is often used. The steroids that will be addressed in this paper are boldenone, trenbolone and drostanolone, as well as their solid forms. For these compounds, the interactions within the crystal lattice will be evaluated using Hirshfeld surfaces that illustrate intermolecular interactions and give suggestive graphical information on the atoms involved in intermolecular interactions. Also, the energies of the crystal lattice were evaluated using the CLP (Coulomb-London-Pauli) method, which evaluates the lattice energies based on atom-atom interactions and provides quantitative information on the types of interactions (Coulombian, polarization, dispersion, repulsion) and of the total lattice energy which is related to the stability of the crystal structures.

Because all the steroids analyzed have carbon rings consisting of five and six members, their conformational analysis was done by evaluating parameters such as asymmetry parameters, pseudo-rotation angle and maximum torsion angle. Both the intermolecular and lattice energy analysis and the conformational analysis were presented in the theory section.

## Boldenone and some boldenone esters

Boldenone (Androsta-1,4-dien-17 $\beta$ -ol-3-one, Fig. 2.1) is a chemical compound that belongs to the class of anabolic-androgenic steroids and occurs naturally in a certain species of aquatic beetle [25]. Boldenone can be seen as a steroid with mild androgenic activity, being derived from testosterone [26, 27]. We focused with the crystallization, the determination of the crystal structure and characterization of five boldenone-based compounds [28], presented in Fig. 2.1. The longer ester chains will have a longer half-life, so the boldenone base will have a half-life of hours, and the duration of action for boldenone cypionate will be several weeks.

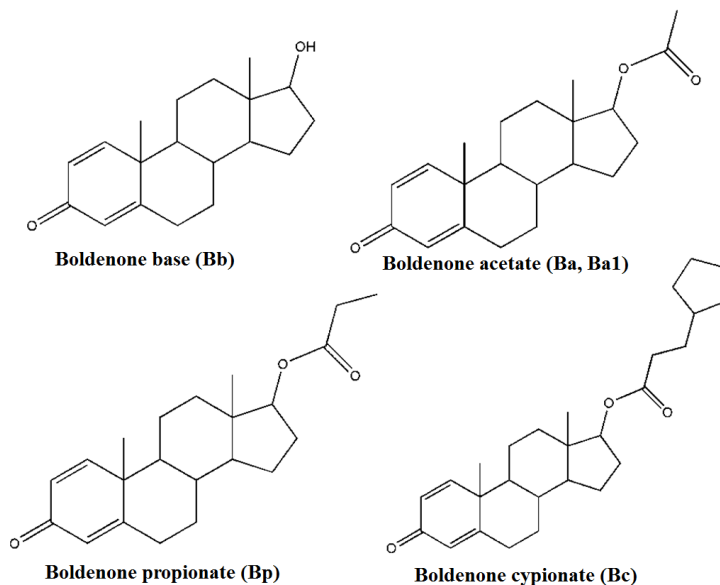


Figure 2.1: Chemical structures of boldenone based compounds

The best single crystals of the compounds were obtained using the following solvents or solvent mixture: acetonitrile for Bb, tetrahydrofuran for Ba, methyl tert-butyl ether for Ba1, Bp in methanol-water ratio 8: 2 and Bc in 2-propanol.

### Crystal structures analysis

The crystal structures for the following chemical compounds from boldenone class were solved: boldenone base, boldenone acetate, boldenone propionate and boldenone cypionate which are shown in Fig 2.2. Boldenone base, Bb has the asymmetric unit

consisting of two molecules of boldenone, while the asymmetric units for Ba, Ba1, Bp and Bc consist of a single molecule (Fig. 2.2).

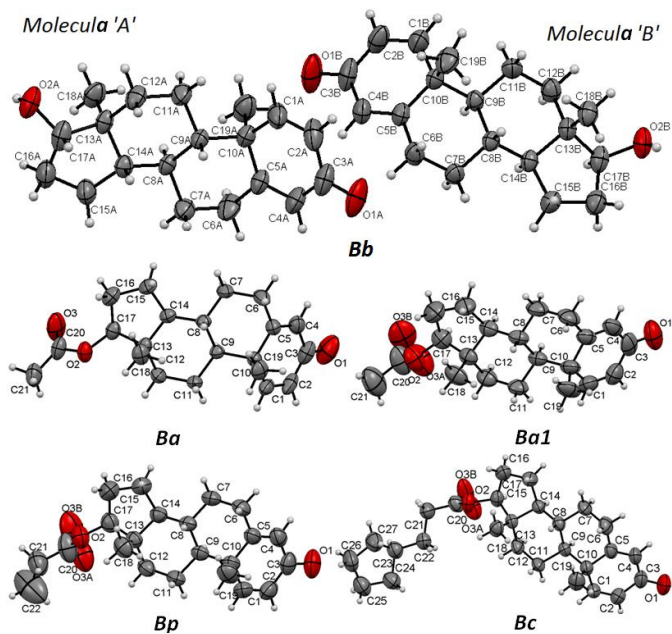


Figure 2.2: Molecular perspectives presented in ORTEP style with atoms as thermal ellipsoids: Bb-boldenone base; Ba-boldenone acetate; Ba1-boldenone acetate (polymorph); Bc-boldenone cypionate

For all studied crystal structures, comparisons between simulated X-ray patterns from single crystals and experimental ones obtained by X-ray powder diffraction show a good fit, which is an indication that the analyzed single crystals are representative for the powders from which they were obtained. In Fig. 2.3 is exemplified for one of the structures: (Ba).

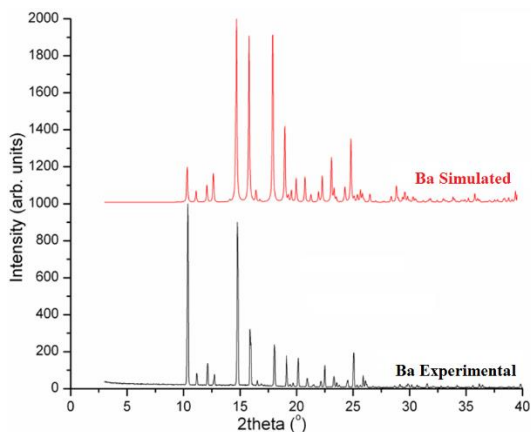


Figure 2.3: Simulated and experimental X-ray diffraction patterns for Ba  
The basic crystallographic details are presented in table 2.1.

Table 2.1: Significant crystallographic details

Compound	Bb (boldenone base)	Ba (boldenone acetate)	Ba1 (boldenone acetate, polymorph)
Empirical formula	$C_{38}H_{52}O_4$	$C_{21}H_{28}O_3$	$C_{21}H_{28}O_3$
Molecular weight	572.80	328.43	328.43
Temperature/K	293	293	293
Crystal system	monoclinic	orthorhombic	orthorhombic
Space group	$P2_1$	$P2_12_12_1$	$P2_12_12_1$
$a/\text{\AA}$	7.08	10.45	31.50
$b/\text{\AA}$	18.64	12.00	8.13
$c/\text{\AA}$	12.31	14.51	7.32
$\alpha/^\circ$	90	90	90
$\beta/^\circ$	90.15	90	90
$\gamma/^\circ$	90	90	90
Volume/ $\text{\AA}^3$	1626	1822	1876
Z	2	4	4
$\rho_{\text{calc}}/\text{g/cm}^3$	1.170	1.197	1.163

Compound	Bp (boldenone propionate)	Bc (boldenone cypionate)
Empirical formula	C <sub>22</sub> H <sub>30</sub> O <sub>3</sub>	C <sub>27</sub> H <sub>38</sub> O <sub>3</sub>
Molecular weight	342.46	410.57
Temperature/K	293	293
Crystal system	monoclinic	orthorhombic
Space group	P2 <sub>1</sub>	P2 <sub>1</sub> 2 <sub>1</sub> 2 <sub>1</sub>
a/Å	7.39	7.62
b/Å	8.23	15.92
c/Å	16.39	19.59
α/°	90	90
β/°	102.09	90
γ/°	90	90
Volume/Å <sup>3</sup>	975	2380
Z	2	4

The description of the crystal structures highlighted the packaging, supramolecular assemblies and synthons based on the intermolecular bonds O-H...O, C-H...H-C, C-H...C and C-H...O for the analyzed boldenone structures (Bb, Ba, Ba1, Bp, Bc). As an example, in Fig. 2.4 intermolecular interactions in boldenone acetate, Ba are presented

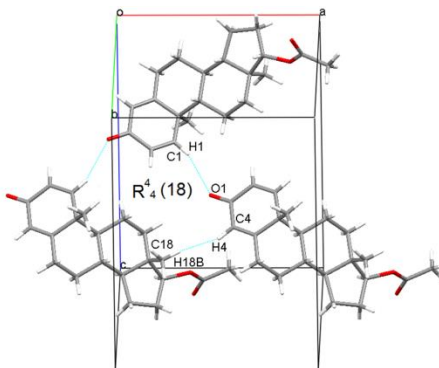


Figure 2.4: Intermolecular interactions in boldenone acetate Ba, along the *ob* axis

The crystal structure of boldenone acetate, Ba consists as an arrangement based on C-H...O and C-H...H-C interactions, building R<sup>4</sup><sub>4</sub>(18) motifs in which three molecules of boldenone acetate are involved (Fig. 2.4). C-H...O interactions are formed between the O1 oxygen of the carbonyl group and the C1 carbon of the A ring.

## Evaluation of lattice energies

Crystal lattice energies were calculated using the classical Coulomb–London–Pauli atom-atom approximation implemented in the CLP program. The total lattice energy and partitioned contributions are shown in table 2.2. It can be seen that the dispersion term dominates all structures, the highest value (-161 kJ/mol), being calculated in Bc due to the fact that for large molecules the dispersion term tends to be significantly higher. The polymorph of boldenone acetate has a slightly less stable crystal structure in terms of energy (-144.1 kJ/mol for Ba1) compared to the starting compound (-147.1 kJ/mol for Ba). Coulomb energy is higher in absolute value in shorter esters, so that Bb that does not have an attached ester has the highest value (-40.3 kJ/mol), due to the classical hydrogen bonds O-H...O, which are stronger than the C-H...O bonds in the other structures.

Table 2.2 CLP lattice energies

Structure	E <sub>coul</sub> (kJ/mol)	E <sub>pot</sub> (kJ/mol)	E <sub>disp</sub> (kJ/mol)	E <sub>atr</sub> (kJ/mol)	E <sub>rep</sub> (kJ/mol)	E <sub>tot</sub> (kJ/mol)
Bb	-40.3	-42.4	-123.6	-206.3	50.4	-155.9
Ba	-30.2	-48.6	-136.1	-214.9	67.8	-147.1
Ba1	-21.3	-45.7	-121.0	-188.0	43.9	-144.1
Bp	-21.3	-43.6	-124.8	-189.7	46.2	-144.1
Bc	-20.1	-54.9	-161.0	-236.0	65.2	-170.8

E<sub>coul</sub>: Coulombic term; E<sub>pot</sub>: polarization; E<sub>disp</sub>: dispersion; E<sub>atr</sub>: attraction (the sum of Coulombic, polarization, dispersion terms); E<sub>rep</sub>: repulsion; E<sub>latt</sub>: CLP crystal lattice energy

## Conformational analysis results

In all studied compounds, ring A adopts planar conformation, rings B and C have chair conformation, while rings D there are as a distorted 13 $\beta$  envelope conformation in Bb molecules and slightly distorted envelope conformation in Ba, Ba1, Bp, Bc. The deviations of the rings from the ideal symmetry are defined by the asymmetry parameters ( $\Delta C_1$ ,  $\Delta C_2$ ) which measure the degree of distortion from the ideal conformation and the value of the maximum torsion angle is approximately 47°. The results for the asymmetry parameters are summarized in table 2.3 and 2.4.

Table 2.3: Calculated asymmetry parameters

Structure	Ring B	Ring C	Ring D
Bb	Molecule A: $\Delta C_s(C5A-C8A)=1.82$	Molecule A: $\Delta C_s(C9A-C13A)=4.88$	Molecule A: $\Delta C_2(C13A-C14A)=9.92$ $\Delta C_s(C13A)=10$
	Molecule B: $C5B-C8B)=1.24$	Molecule B: $C9B-C13B)=3.77$	Molecule B: $\Delta C_2(C13B-C14B)=12.83$ $(C13B)=8.61$
Ba	$\Delta C_s(C5-C8)=0.709$	$\Delta C_s(C9-C13)=3.214$	$\Delta C_2(C13-C14)=21.87$ $\Delta C_s(C13)=1.96$
Ba1	$\Delta C_s(C5-C8)=3.47$	$\Delta C_s(C9-C13)=4.77$	$\Delta C_2(C13-C14)=15.69$ $\Delta C_s(C13)=6.72$
Bp	$\Delta C_s(C5-C8)=2.73$	$\Delta C_s(C9-C13)=2.25$	$\Delta C_2(C13-C14)=19.3$ $\Delta C_s(C13)=4.1$
Bc	$\Delta C_s(C5-C8)=2.86$	$\Delta C_s(C9-C13)=3.43$	$\Delta C_2(C13-C14)=14.28$ $\Delta C_s(C13)=7.26$

Table 2.4: Pseudorotation angle, P and maximum torsion angle  $\tau_m$  ( $^\circ$ )

Structure	Bb (Mol A)	Bb (Mol B)	Ba	Ba1	Bp	Bc
P	7.68	9.64	15.75	11.2	14.57	10.8
$\tau_m$	47.32	47.81	49.45	48.42	49.38	47.59

### Fingerprint and Hirshfeld analysis

The dominant contributions of the H... H, C... H and O... H contacts (table 2.5) indicate that van der Waals interactions and hydrogen bonds stabilizes the packing of crystals. Hirshfeld and fingerprint surfaces were generated for all structures but will only be exemplified for boldenone acetate, Ba.

Table 2.5: Contributions to Hirshfeld surfaces

Structure	O...H/H...O	C...H/H...C	H...H
Molecule A of Bb	17.9%	7.4%	74.7%
Molecule B of Bb	18.3%	7.8%	73.7%
Ba	23.2%	8.4%	68.4%
Bal	25.6%	3.9%	69.9%
Bp	23.8%	4.6%	70.7%
Bc	17.8%	5.6%	76.6%

In Fig. 2.5 arrow 1 indicates the interaction C1-H1...H4-C4, 2 and 3 represent the interaction C1-H1...O1, the donor and acceptor being alternately inside and outside the Hirshfeld surface.

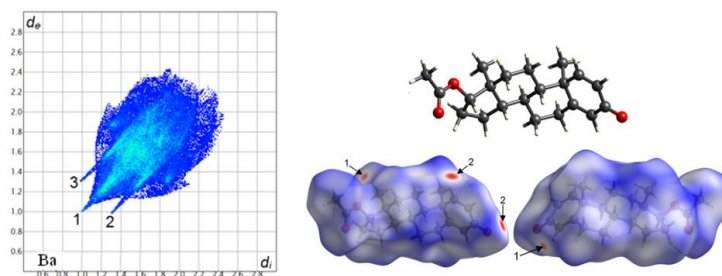


Figure 2.5: Hirshfeld surface and fingerprint plot for Ba indicating the intermolecular contacts denoted as follows: H...H (1), O...H (2), H...O (3)

### Trenbolone and some trenbolone esters

Trenbolone (Fig. 2.6) is a compound, derived from the nandrolone that differs from nandrolone by adding a double bond between C10-C9 and C11-12. Several esterified forms of trenbolone are available, including trenbolone acetate, trenbolone hexahydrobenzylcarbonate (parabolan), both of which have had clinical and veterinary use [22], and trenbolone enanthate, which is dedicated to athletes [22] and for scientific purposes [29]. From the class of trenbolone-based compounds (Fig. 2.7), the crystal structure of trenbolone acetate and hexahydrobenzylcarbonate were solved single crystal X-ray diffraction. Also, the crystal structure for enanthate trenbolone was solved from powder [30]. Quantitative analysis of intermolecular interactions was done by Hirshfeld

analysis, and lattice energies were evaluated in the Coulomb-London-Pauli approximation. All calculations for trenbolone base were performed on the CIF file deposited in CSD [31].

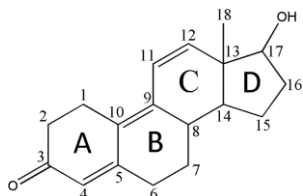


Figure 2.6: Structural scheme of trenbolone, showing the numbering system

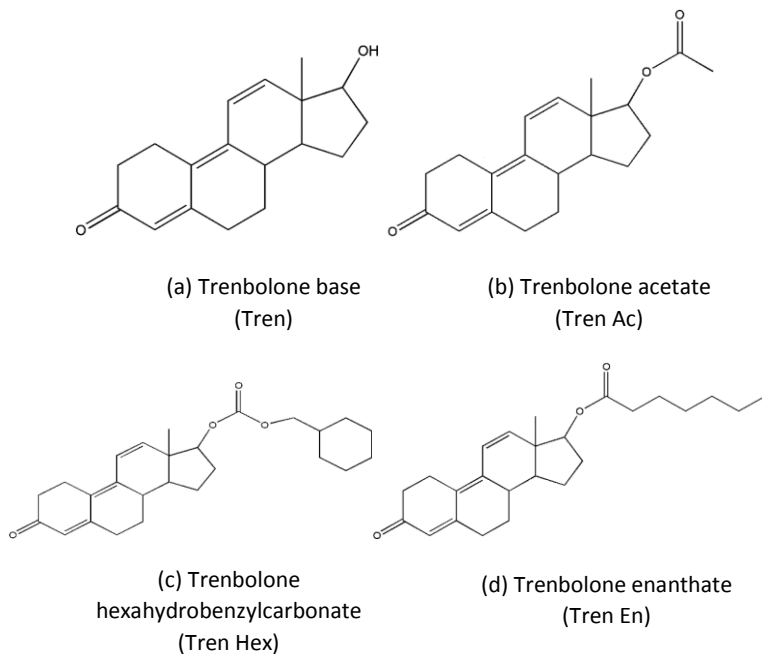


Figure 2.7: Structural schemes of investigated compounds based on trenbolone

Comparisons between powder and simulated X-ray diffraction patterns are shown in Fig. 2.8 indicating a good agreement between them, good purity and structural homogeneity.

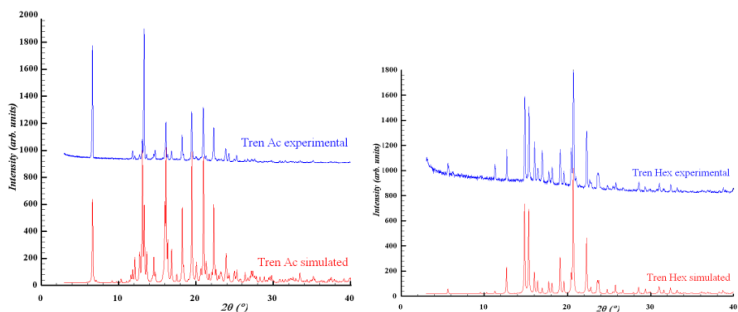


Figure 2.8: Simulated and experimental diffraction patterns: Tren Ac; Tren Hex  
**Crystal structure determination of trenbolone enanthate from X-ray powder diffraction**

Since it was not possible to obtain single crystals for trenbolone enanthate, the method for solving the crystal structure on powders was used with the methodology described in Chapter 1. The results are summarized in table 2.6 and the match between the calculated and experimental patterns in Fig. 2.9.

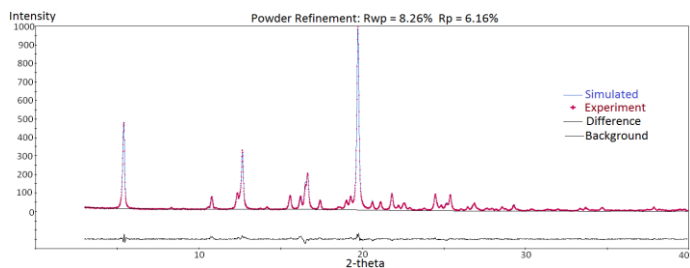


Figure 2.9: Simulated and experimental patterns from Rietveld refinement

Table 2.6: Structural parameters of trenbolone enanthate

Chemical formula	$C_{25}H_{34}O_3$
Molecular weight (g/mol)	360.53
Crystal system	monoclinic
Space group	$P2_1 (4)$
$Z$	2
$a$ (Å)	9.74
$b$ (Å)	13.97
$c$ (Å)	16.38
$\beta$ (°)	90.42
$V$ (Å <sup>3</sup> )	2229
$R_{wp}$ (%)	8.26
$\rho_{calc}$ g/cm <sup>3</sup>	1.137

### Crystal structures descriptions of trenbolone-based compounds

The basic crystallographic information with regard to crystal structures are presented in table 2.7.

Table 2.7: Crystallographic data for single crystals (Tren Hex and Tren Ac)

Compound	Tren Hex	Tren Ac
Empirical formula	C <sub>26</sub> H <sub>32</sub> O <sub>4</sub>	C <sub>20</sub> H <sub>24</sub> O <sub>3</sub>
Molecular weight	408.51	312.39
Temperature/K	293	293
Crystal system	monoclinic	monoclinic
Space group	P2 <sub>1</sub>	P2 <sub>1</sub>
a/Å	9.37	9.36
b/Å	7.79	13.97
c/Å	15.86	26.66
$\alpha$ /°	90	90
$\beta$ /°	98.94	95.43
$\gamma$ /°	90	90
Volume/Å <sup>3</sup>	1145	3474
Z	2	8
$\rho_{\text{calc}}/\text{cm}^3$	1.184	1.195

In thesis, the crystal structures for four trenbolone-based compounds have been described, but this summary will present only the structure for trenbolone acetate.

Trenbolone acetate has a rather unusual asymmetric unit, which consists of four independent molecules A, B, C, D (Fig. 2.9a) and eight in the unit cell (Fig. 2.9b). The eight molecules are linked two by two by a 2nd order screw axis, having the same notation. The crystal structure is stabilized by C-H...O and C-H... $\pi$  bonds. The C ...O interactions are as follows: C2B-H...O1A, C16-H...O3B, C2C-H...O1D, C16A-H...O1B, C16D-H...O1C, C1D-H...O3D, C16D-H...O1C, while the C-H... $\pi$  interactions are: C2B-H...C11A and C2C-H...C11D. The suffixes A, B, C, D indicates the molecules of which the respective atoms belong (Fig. 2.9b). Overlapping the four molecules in the asymmetric unit, it is observed that the pairs A-D and B-C are very similar from a geometric point of view.

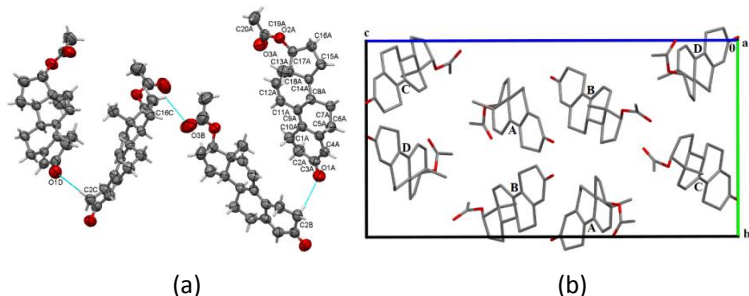


Figure 2.9: Asymmetric unit of trenbolone acetate (a); Molecular arrangement of trenbolone acetate in the elementary cell (b)

### Hirshfeld and fingerprint surfaces analysis

Hirshfeld surfaces and intermolecular interactions were calculated for all compounds studied: trenbolone base, trenbolone acetate (four molecules in the asymmetric unit), trenbolone hexahydrobenzylcarbonate and trenbolone enanthate, but in this summary are shown only for trenbolone enanthate (table 2.8 and Fig. 2.10).

Table 2.8: Intermolecular contacts shorter than the sum of van der Waals radii

Molecule	Contact	d(C-H) (Å)	d(H...A) (Å)	d(D...A) (Å)	<(D-H...A) (°)
Tren En Molecule A	C2B-H2BB...O1A	0.97	2.545	3.384	144.75
	C2B-H2BA...C11A	0.97	2.856	3.722	149.23
	C11B-H11B...O3A	0.93	2.696	3.595	162.88
	C16A-H16B...O1B	0.97	2.583	3.443	147.83
Tren En Molecule B	C2B-H2BB...O1A	0.97	2.545	3.384	144.75
	C2B-H2BA...C11A	0.97	2.856	3.722	149.23
	C11B-H11B...O3A	0.93	2.696	3.595	162.88
	C16A-H16B...O1B	0.97	2.583	3.443	147.83

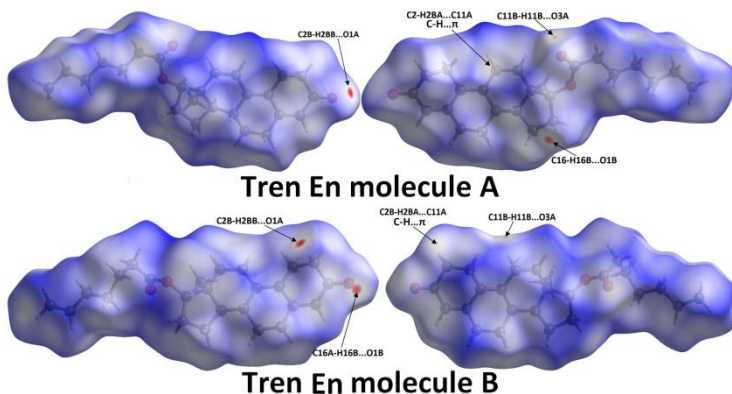


Figure 2.10: Hirshfeld surfaces for Tren En

### Crystal lattice energies analysis

The total and partitioned lattice energies were calculated in the atom-atom, Coulomb-London-Pauli approximation and are shown in table 2.9. It is observed that long esters have lower energies, resulting in greater structural stability. The Coulomb component is more important in the Tren because this crystal structure has strong hydrogen bonds compared to other structures. Dominant value of the dispersion components is a common feature.

Table 2.9: CLP lattice energies

Structure	$E_{\text{coul}}$ (kJ/mol)	$E_{\text{pol}}$ (kJ/mol)	$E_{\text{disp}}$ (kJ/mol)	$E_{\text{atr}}$ (kJ/mol)	$E_{\text{rep}}$ (kJ/mol)	$E_{\text{tot}}$ (kJ/mol)
Tren	-40.0	-38.8	-130.0	-208.8	59.8	-149.1
Tren Ac	-25.7	-44.2	-129.7	-199.6	51.4	-148.2
Tren Hex	-10.3	-48.8	-163.6	-222.7	59.9	-162.8
Tren En	-24.6	-52.9	-158.7	-236.2	55.8	-180.7

$E_{\text{coul}}$ : Coulombic term;  $E_{\text{pol}}$ : polarization;  $E_{\text{disp}}$ : dispersion;  $E_{\text{atr}}$ : attraction (the sum of Coulombic, polarization, dispersion terms);  $E_{\text{rep}}$ : repulsion;  $E_{\text{latt}}$ : CLP crystal lattice energy

2D fingerprint diagrams were generated and analyzed for all structures but in this summary are presented only for trenbolone and trenbolone hexahydrobenzylcarbonate (Fig. 2.11). Fingerprint plots were evaluated, highlighting intermolecular contacts and quantitatively percentage contribution for different types of interactions are summarized in Table 2.10

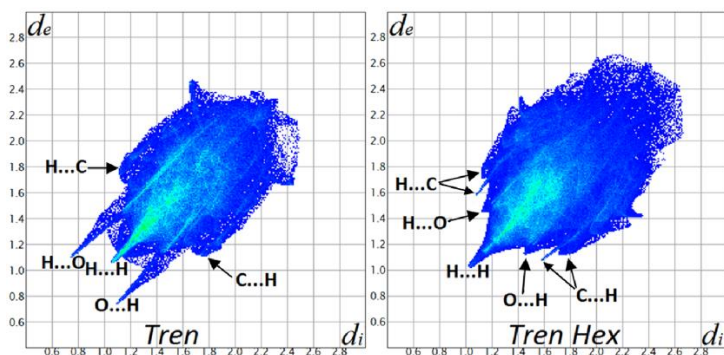


Figure 2.11: Particular fingerprint plots for Tren and Tren Hex

Table 2.10. Contributions (%) to the Hirshfeld surfaces for different contacts

Structure	H...H	O...H/H...O	C...H/H...C	C...O/O...C	O...O	C...C
Tren	71.4	19.5	8.2	-	-	0.8
Molecule A, Tren Ac	70.1	19.7	9.4	0.3	-	0.5
Molecule B, Tren Ac	70.0	20.9	9.0	0.1	0.1	-
Molecule C, Tren Ac	68.0	23.0	8.9	0.1	-	-
Molecule D, Tren Ac	70.2	19.0	10.1	0.2	0.1	0.4
Tren Hex	66.4	19.7	13.8	0.1	-	-
Molecule A, Tren En	76.0	16.4	6.8	0.4	-	0.4
Molecule B, Tren En	78.1	13.8	8.1	-	-	-

### Conformational analysis

For all trenbolone molecules studied, the five-membered D-rings can be approximated as distorted  $13\beta$  envelope conformations, while the geometries for the six-membered A, B, C rings differ from one structure to another. Conformational analysis for rings with six carbons (A, B and C) and five (D) was made by calculating  $\Delta C_s$ ,  $\Delta C_2$ ,  $P$  and  $\tau_m$  to highlight their deformation from the ideal configuration and are presented in table 2.11, atom notations being according to Fig. 2.6. The least deformed rings are found in the Tren Hex, the A ring being almost planar and to a lesser extent in the Tren structure.

Table 2.11: Conformational parameters describing the rings

Structure	Ring A $\Delta C_s$ (C1-C4)	Ring B $\Delta C_s$ (C7-C10)	Ring C $\Delta C_s$ (C11-C14)	Ring D		Ring D	
				$\Delta C_s$ (C13)	$\Delta C_2$ (C16)	P	$\tau_m$
Tren	24.66	0.36	1.57	7.57	13.69	10.58	47.78
Tren Ac-Mol A	17.21	12.31	8.04	14.48	6.07	4.28	49.60
Tren Ac-Mol B	18.63	9.81	9.93	10.05	10.21	7.76	47.14
Tren Ac-Mol C	18.45	13.19	11.90	2.28	20.55	15.75	47.39
Tren Ac-Mol D	17.27	13.26	5.47	15.59	4.36	2.95	49.39
Tren Hex	2.70	4.08	2.94	7.10	14.77	11.02	48.48
Tren En-Mol A	17.07	14.38	6.79	14.43	6.24	4.30	49.71

The conformation in the D-rings, evaluated by pseudorotation and the maximum torsion angle (table 2.11) show that the  $\tau_m$  values are quite close to the common value of  $47^\circ$  found in the D-rings of some compounds from the same family [32].

### Drostanolone propionate and its polymorphs

Drostanolone propionate (2-methyl-4,5 $\alpha$ -dihydrotestosterone 17-propionate), known as masteron (Fig. 2.11b), is a steroid derived from dihydrotestosterone (Fig. 2.11a) [25, 27]. This agent acts in the same way as any anabolic steroid, being an androgen receptor agonist [22]. From a medical point of view, it has been used in the treatment of breast cancer [25]. Will be approached three polymorphs of drostanolone propionate [33].

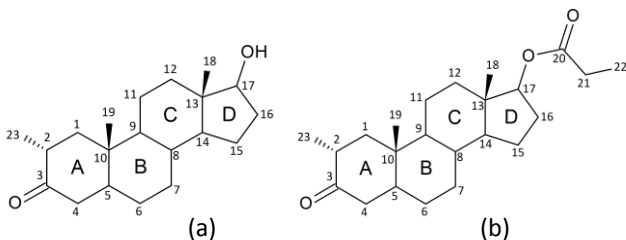


Figure 2.11: Chemical scheme of drostanolone (a) and drostanolone propionate (b) showing the numbering system of atoms.

### Crystal structures for drostanolone propionate polymorphs and their description

Suitable needle-shaped single crystals for X-ray experiments were obtained for the polymorph Drost 2 in ethanol solution by slow evaporation method and plate shaped crystals in acetone solution for polymorph denoted Drost 3. No suitable single crystals

were obtained for the start compound (polymorph Drost 1) and therefore the structure was solved from powders.

The chemical configurations of drostanolone and drostanolone propionate are shown in Fig. 2.11. For Drost 3 there are two molecules in the asymmetric unit (denoted by molecule A and molecule B). The most important crystallographic data are described in table 2.12.

Table 2.12: Single crystal structural data

Compound	Drost 2 (Etanol)	Drost 3 (Acetonä)
Empirical formula	C <sub>23</sub> H <sub>36</sub> O <sub>3</sub>	C <sub>23</sub> H <sub>36</sub> O <sub>3</sub>
Molecular weight	360.52	360.52
Temperature/K	293	293
Crystal system	monoclinic	monoclinic
Space group	P2 <sub>1</sub>	I2
a/Å	11.23	11.87
b/Å	7.43	7.42
c/Å	12.50	48.63
$\alpha$ /°	90	90
$\beta$ /°	93.64	96.66
$\gamma$ /°	90	90
Volume/Å <sup>3</sup>	1042	4260
Z	2	8
$\rho_{\text{calc}}/\text{cm}^3$	1.149	1.124

Crystal structures, packings descriptions of the molecules in the unit cell, hydrogen bonds and other intermolecular contacts were analyzed for all polymorphs but in this summary is presented only for Drost2 polymorph.

The unit cell of the Drost 2 polymorph contains two molecules related by a second-order screw axis connected by C5-H...H-C12 contact, formed between carbon C5, which is common to rings A and B, and carbon C12 of ring C. The supramolecular assembly is further extended by translations and forms an arrangement parallel to the *ob* direction. At the same time, along the *oc* axis, an infinite arrangement of molecules is formed, which are linked between the carbonyl oxygen O3 and the methyl group C19 by the hydrogen bond C19-H...O3, as shown in Fig. 2.12.

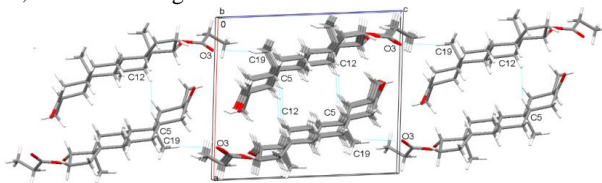


Figure 2.12: Packaging scheme of molecules in Drost 2

Crystal structure determination of polymorph Drost 1 from crystalline powders was performed by the methods described in Chapter 1.

The crystallographic data and the final match between the calculated and measured diffraction patterns show a good agreement, with  $R_{wp} = 5.65\%$  (table 2.13 and Fig. 2.13).

Table 2.13: Crystallographic data for polymorph Drost 1

Chemical formula	$C_{23}H_{36}O_3$
Molecular weight (g/mol)	360.53
Crystal system	orthorhombic
Space group	$P 2_1 2_1 2_1 (19)$
Z	4
a (Å)	27.25
b (Å)	12.07
c (Å)	6.41
V (Å <sup>3</sup> )	2111
$R_{wp}$ (%)	5.64

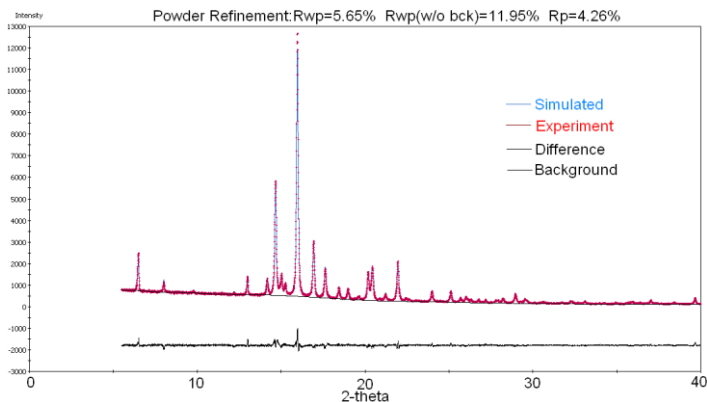


Figure 2.13: Fitting between experimental and calculated diffraction patterns

### Hirshfeld surfaces and fingerprint plots analysis

The front and rear views of the three-dimensional Hirshfeld surfaces were generated for all drostanolone propionate structures but we will present only for polymorph Drost 2. Fig. 2.14 shows the frontal view of the Hirshfeld surface, respectively, the back view of the Drost 2 polymorph and the intermolecular interactions shorter than the sum of the van der Waals radii presented as arrows. Each number illustrated on the Hirshfeld surface has the interaction geometry detailed in table 2.14.

Table 2.14: Shorter intermolecular contacts than the sum of van der Waals radii (Å).

Structure	Contact	d(C-H)	d(H...A)	d(D...A)
Drost 2	C19-H19B...O3	0.96	2.687	3.622
	C12-H12A...H5-C5	0.97/ 0.98	2.341	4.047

The fingerprint plots breakdown shows that in all three crystals, the H...H interactions have a higher participation compared to the other contacts: the O...H/H...O interactions which represent the second place as participation and the C...H/H...C much less significant. The percentage contributions to the Hirshfeld surfaces for the studied crystals are represented in table 2.14. The high percentage of H...H, O...H and C...H inter-contacts indicates that the structures are based on weak van der Waals interactions, which ensure the packing of the crystals [34].

Table 2.14: Contribution to Hirshfeld surfaces of different interactions

Structure	H...H	O...H/H...O	C...H/H...C	C...O/O...C	O...O	C...C
Drost 1	83.2%	16.0%	0.5%	0.3%	-	-
Drost 2	83.3%	14.6%	0.9%	0.5%	0.8%	-
Drost 3 Mol. A	83.4%	14.3%	1.1%	0.6%	0.6%	-
Drost 3 Mol. B	82.0%	16.7%	0.5%	0.5%	0.2%	0.1%

### Lattice energies evaluation by Coulomb-London-Pauli method

By the CLP method, which is based on atom-atom potentials, it was shown that the formation of two polymorphs of drostanolone propionate led to structures with similar energies being shown in Table 2.15a (-156.3 kJ/mol in Drost 1; -159.2 kJ/mol in Drost 2 and -151.6 kJ/mol in Drost 3, respectively). Table 2.14a also shows the fraction of different lattice energies components.

Table 2.15a.  $E_{\text{coul}}$ : Coulombic term;  $E_{\text{pol}}$ : polarization;  $E_{\text{disp}}$ : dispersion;  $E_{\text{att}}$ : attraction (the sum of Coulombic, polarization, dispersion terms);  $E_{\text{rep}}$ : repulsion;  $E_{\text{latt}}$ : CLP crystal lattice energy

Structure	$E_{\text{coul}}$	$E_{\text{pol}}$	$E_{\text{disp}}$	$E_{\text{att}}$	$E_{\text{rep}}$	$E_{\text{latt}}$
Drost 1	-16.0	-54.1	-130.4	-200.5	44.2	-156.3
Drost 2	-10.3	-56.5	-139.4	-206.2	48.7	-159.2
Drost 3	-13.0	-55.2	-134.7	-202.9	51.4	-151.6

The dispersion and total CLP energy values were compared with the results obtained based on the DFT method (table 2.15b) and a reasonable concordance is found (see comparison between table 2.15a and 2.15b for  $E_{\text{disp}}$  and  $E_{\text{latt}}$ ).

Table 2.15b: lattice and dispersion DFT energies (kJ/mol)

<b>Structura</b>	<b>E<sub>disp</sub>(N<sup>∞</sup>)</b>	<b>E<sub>latt</sub>(N<sup>∞</sup>)</b>
Drost 1	-125.9	-142.6
Drost 2	-138.3	-151.7
Drost 3	-119.7	-137.7

Both methods suggest that the main attractive forces that hold the crystal cohesion are the dispersion effects.

### Conformational analysis

Rings A, B and C of the steroid skeletons were found to adopt chair conformation, while Rings D adopted a C13 envelope conformation in all three structures. The distortion of rings were described by the asymmetry parameter  $\Delta C_s$  [21]. The calculated values show that the geometry of the A, B and C rings for all polymorphs is close to the ideal chair configuration (table 2.16). The maximum torsion parameter,  $\tau_m$  (Table 2.17), proved to be relatively constant and close to 47°, which is a common value found in all D-rings for such compounds [35].

Table 2.16: Asymmetry parameters values in the studied polymorphs.

	<b>Mirror plane</b>	<b>Drost 1</b>	<b>Drost 2</b>	<b>Drost 3-Mol A</b>	<b>Drost 3-Mol B</b>
Ring A	$\Delta C_s$ (C3-C10)	1.22	2.72	0.69	2.43
	$\Delta C_s$ (C4-C1)	1.12	0.90	2.93	2.51
	$\Delta C_s$ (C5-C2)	1.27	1.85	3.41	4.49
	Media $\Delta C_s$	1.20	1.82	2.34	3.14
Ring B	$\Delta C_s$ (C5-C8)	1.46	2.67	3.43	2.28
	$\Delta C_s$ (C6-C9)	4.50	3.37	0.30	4.33
	$\Delta C_s$ (C7-C10)	3.73	0.75	3.14	6.13
	Media $\Delta C_s$	3.23	2.27	2.29	4.24
Ring C	$\Delta C_s$ (C9-C13)	3.49	2.00	2.26	2.35
	$\Delta C_s$ (C8-C12)	4.21	8.62	6.94	3.49
	$\Delta C_s$ (C14-C11)	0.84	6.86	8.79	5.62
	Media $\Delta C_s$	2.85	5.83	5.99	3.82



from ethanol:water (1:5), heated to 40° C for 24 hours followed by slow cooling at room temperature; (b) by heating the ostarine powder to 125° C followed by slow cooling to room temperature. Both methods gave the same polymorph.

### Spectroscopic (FT-IR) and thermal (DTA/TGA) analysis

The configurations of the asymmetric units resulting from the X-ray diffraction for Os, AND and Os-P1 are shown in Fig. 3.2 where the specific functional groups are observed and have been highlighted by FTIR analysis.

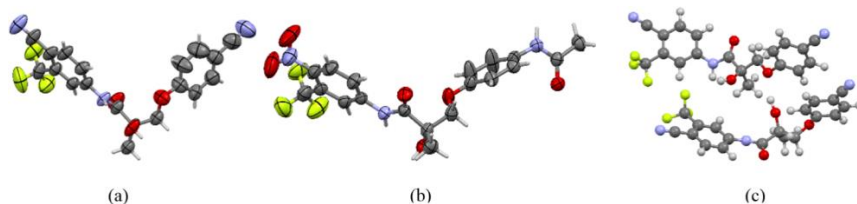


Figure 3.2: Molecular view for ostarine (a), andarine (b), Os-P1 ostarine polymorph (c) showing the two molecules that form the asymmetric unit.

The vibrational spectra (Fig. 3.3) for ostarine (Os) and its polymorph (Os-P1) being very similar lead us to the conclusion that Os-P1 is a polymorph and not another solid form because no additional bands appear but only a slight shift is found.

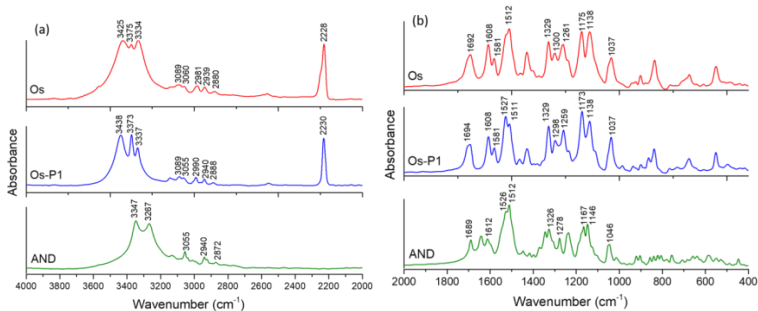


Figure 3.3: FT-IR spectra for Os, Os-P1 și AND

The Os-P1 polymorph obtained by heating to 120° C shows a similarity of the DTA/TGA curves (Fig. 3.3) with those of the starting compound (Os), except that there is no phase change at 95.2° C. The melting point is 140,53° C and the decomposition is around 371° C.

For andarine (AND) no phase transformations are reported, the endothermic signal occurring around 156° C represents the melting point of compound and has a higher value

than ostarine. Decomposition and degradation take place in two stages around 356° C and 411° C, respectively.

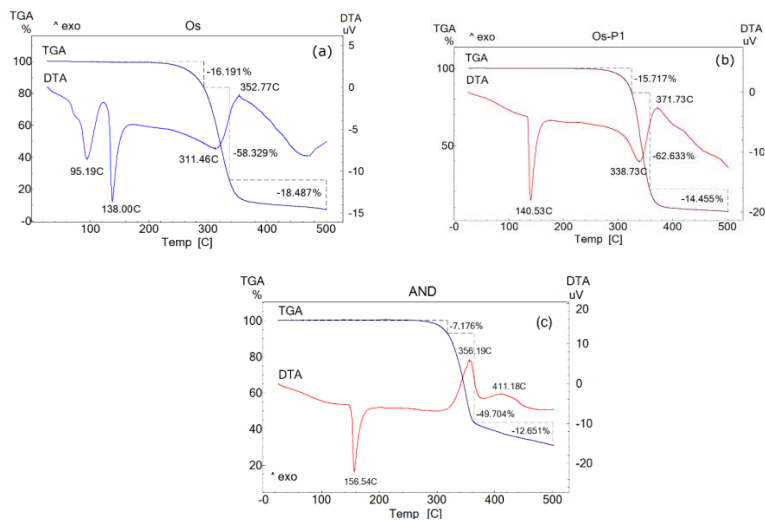


Figure 3.3: DTA/TGA curves: (a) Os, (b) Os-P1, (c) AND

### Crystal structures analysis of Os and AND solved from single crystals

The basic crystallographic data for Os and AND are given in table 3.1.

Table 3.1. Basic crystallographic data from single crystals

Structure	Os (ostarine)	AND (andarine)
Empirical formula	$C_{19}H_{14}F_3N_3O_3$	$C_{19}H_{18}F_3N_3O_6$
Molecular weight	389.33	441.36
Crystal system/Space group	Monoclinic, $P2_1$	Tetragonal, $P4_22_12$
Temperature/K	293	293
$a, b, c$ (Å)	12.01, 5.40, 16.13	19.03, 19.03, 10.95
$\alpha, \beta, \gamma$ (°)	90, 98.47, 90	90, 90, 90
$V$ (Å <sup>3</sup> )	1036	3970
Z	2	8

The molecular self-assembly stability of ostarine (Os) is ensured by two hydrogen bonds O2-H...N3 where O2 is the donor atom and N3 is acceptor, respectively N2-H...O3 where N2 is the donor atom and O3 the acceptor (Fig. 3.4 and table 3.2). Ostarine

molecules are linked by hydrogen bonds both along the direction of *oa* and *ob* axis, forming a two-dimensional network in the *aob* plane (Fig. 3.4).

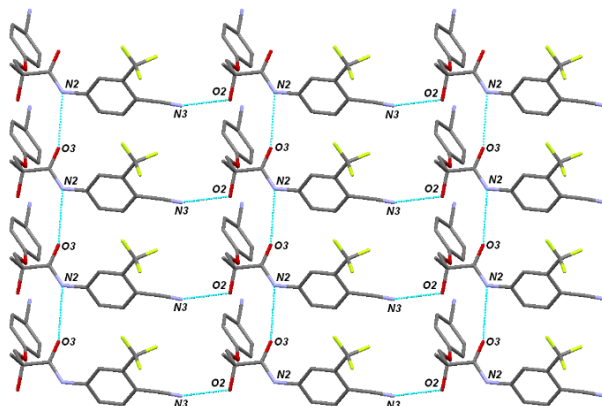


Figure 3.4: Highlighting hydrogen bonds for ostarine in the *aob* plane

Table 3.2: Geometry of hydrogen bonds for ostarine (Å, °)

D-H...A	D-H	H...A	D...A	<(D-H...A)
O2-H...N3	0.820	1.999	2.816	174.9
N2-H...O3	0.860	2.430	3.168	144.3

In the case of the andarine structure, there are two hydrogen bonds, namely: N1-H...O4, which binds a pairs of two molecules together, these pairs are in further linked to other pairs by the O3-H...O1 hydrogen bonds. This arrangement continues further and in this way the molecules are interconnected through an infinite network (Fig. 3.5b and table 3.3). The supramolecular structural unit for andarine consists of two molecules that are connected to each other by the N1-H...O4 hydrogen bond forming a  $R_2^2(22)$  type heterosynthon (Fig. 3.5a). These synthons are connected to each other by bifurcated O3-H...O1 bonds, forming a three-dimensional network, four such interconnected synthons visualized along the *oc* direction are shown in Figs. 3.5b.

Table 3.3: Geometry of hydrogen bonds for andarine (Å, °)

D-H...A	D-H	H...A	D...A	<(D-H...A)
O3-H...O1	0.820	2.091	2.908	174.15
N1-H...O4	0.860	2.115	2.922	156.09

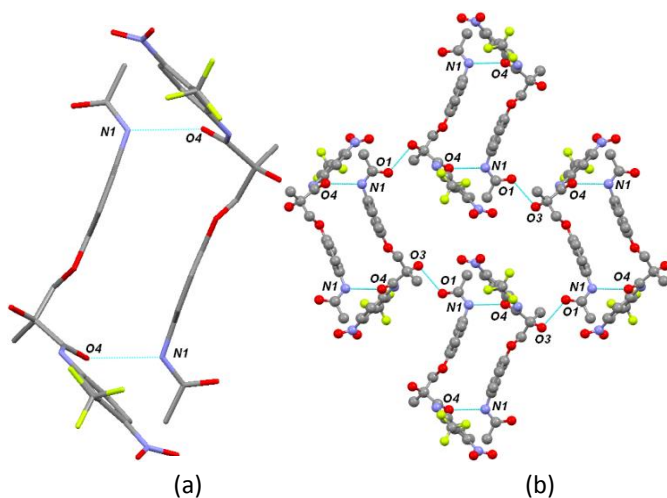


Figure 3.5: Highlighting of heterosinton  $R^2_2(22)$  for andarine (a);  
Supramolecular view along the  $oc$  direction(b)

The experimental X-ray powder diffraction patterns and simulated from single crystals are very similar, which shows that the single crystals are representative for the powders from which they were obtained. The packing over an extended domain of ostarine, which shows a larger number of molecules in the crystal, highlights the fact that the crystal structure has voids in the form of a parallelogram with an angle of  $98.47^\circ$  (Fig. 3.6).

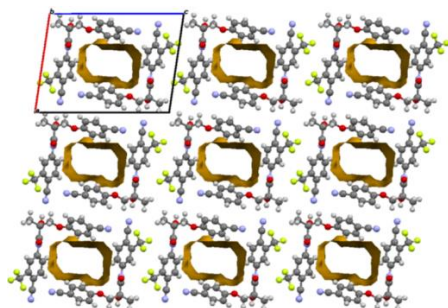


Figure 3.6: Highlighting crystal voids along the  $ob$  axis in Os

As it was not possible to grow suitable crystals from the ostarine polymorph, Os-P1 for single crystal X-ray diffraction experiment, the solution of the crystal structure by powder

diffraction was approached, the results obtained being given in table 3.4 and the comparison between the experimental X-ray diffraction patterns and calculated is shown in Fig. 3.7.



Figure 3.7: Comparison of the experimental pattern with the calculated one

#### Calculation of CLP lattice energy

Lattice energies for ostarine, andarine and the ostarine polymorph Os-P1 are shown in table 3.5. The formation of the polymorph due to heating led to a less energetically stable crystal structure than the starting ostarine, having a lattice energy of -128.4 kJ/mol compared to the starting sample (-149.4 kJ/mol).

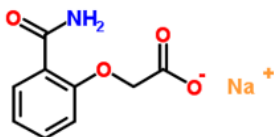
Table 3.5: CLP energies (kJ/mol)

Structure	$E_{\text{coul}}$	$E_{\text{pol}}$	$E_{\text{disp}}$	$E_{\text{att}}$	$E_{\text{rep}}$	$E_{\text{latt}}$
Os	-60.7	-48.9	-144.5	-251.1	106.3	-149.4
Os-P1	-13.0	-56.8	-180.1	-249.9	121.6	-128.4
AND	-76.9	-75.0	-206.8	-357.7	109.1	-249.7

$E_{\text{coul}}$ : Coulombic term;  $E_{\text{pol}}$ : polarization;  $E_{\text{disp}}$ : dispersion;  $E_{\text{att}}$ : attraction;  $E_{\text{rep}}$ : repulsion;  $E_{\text{latt}}$ : CLP crystal lattice energy

#### 4. Structural, spectroscopic and theoretical studies of sodium (2-carbamoylphenoxy) acetate salt

The (2-carbamoylphenoxy) sodium acetate salt, with the chemical formula  $\text{C}_9\text{H}_8\text{NNaO}_4$  (Scheme 4.1), produced under the name of algamon [39], is the salt of the active substance of o-carbamoyl-phenoxyacetic acid, used for its analgesic activity [40].



Scheme 4.1: Molecular scheme of algamon

The crystal structure of algamon was determined by single crystal X-ray diffraction (Table 4.1) and its supramolecular characteristics were investigated [41].

Table 4.1: Basic crystallographic data for algamon

Compound	algamon
Empirical formula	$C_{36}H_{34}N_4Na_4O_{17}$
Molecular weight	886.63
Temperature/K	293
Crystal system	triclinic
Space group	P-1
a/Å	10.85
b/Å	13.62
c/Å	13.85
$\alpha/^\circ$	103.77
$\beta/^\circ$	103.72
$\gamma/^\circ$	100.06
Volume/Å <sup>3</sup>	1873
Z	4
$\rho_{calc}/cm^3$	1.571

Because there are four Na cations and four o-carbamoyl-phenoxyacetic acid (CBA) molecules in the unit cell, they were overlapped to highlight the differences between them (Fig. 4.1). It can be seen that three of the four molecules have similar configuration, one of them being slightly different.

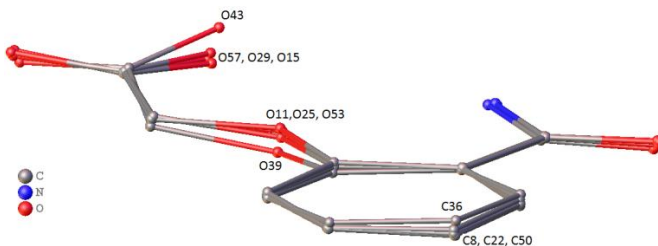


Figure 4.1: Overlap of the four molecules that form the asymmetric unit

Sodium cations are coordinated with oxygen atoms, three Na atoms are six coordinated and one Na atom is five coordinated. By omitting the sodium cations in the structure, it is observed that the crystal structure can be reduced to three  $R_2^2(18)$  type synthons connected by the N-H...O and O-H...O hydrogen bonds between the (2-carbamoylphenoxy) acetate anions (Fig. 4.2).

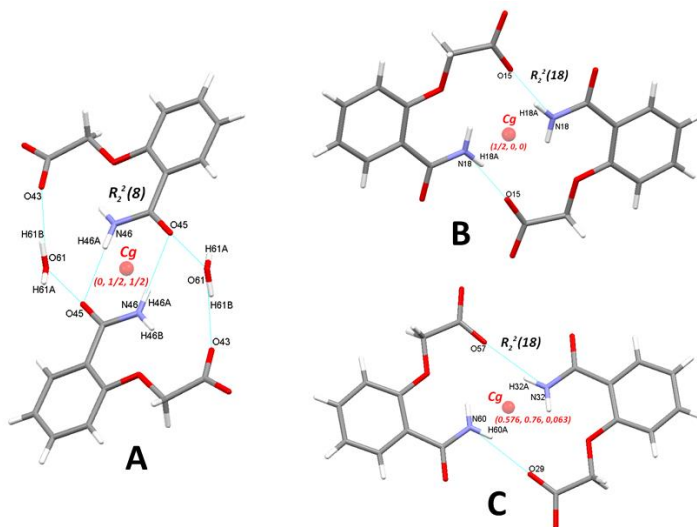


Figure 4.2: Supramolecular synthons and centroid positions (Cg) in the cell

Hirshfeld analysis for all four CBA and water molecules revealed that the strongest interactions are hydrogen bonds, which contribute to the formation of supramolecular synthones and the interactions between oxygen atoms and Na cations.

Being the salt of an active substance in the group of salicylic acid derivatives, namely o-carbamoyl-phenoxyacetic acid, it is interesting to investigate the influence of hydrochloric acid on the structure of sodium salt.

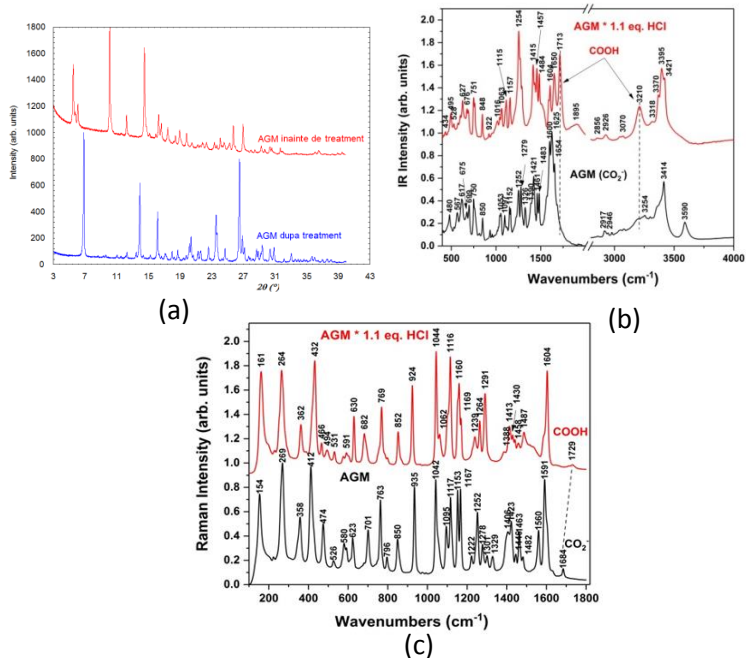


Figure 4.3: X-ray diffraction (a), FT-IR (b); Raman (c) spectra for algamon before and after treatment with 1: 1.1 molar ratio between salt and HCl

From Fig. 4.3a, it can be seen that after the hydrochloric acid treatment a new structure was obtained and there are no traces of the starting material at all. Vibration data (both FT-IR and Raman) indicate the transformation of the sodium salt into the corresponding acid: the appearance of new bands in the IR spectra, at 1713 and 3210  $\text{cm}^{-1}$ , assigned C=O and OH that come from the vibrations of the  $-\text{COOH}$  group (Fig. 4.3b) and the displacement of the asymmetric stretching vibration of  $\text{CO}_2^-$  at a higher frequency after the formation of COOH (from 1684 to 1729  $\text{cm}^{-1}$ ) [42].

## 5. Solid forms of the diuretic compound: 4-chloric salicylic acid-5-sulfonamide

Pharmaceutical solids are used as polymorphs, salts, hydrate solvates and cocrystals [43]. Each crystalline form for a particular pharmaceutical compound has unique properties such as bioavailability and solubility [44]. A molecular cocrystal consists of at least two different solid compounds, which form a crystal structure [45].

4-Chloric salicylic acid-5-sulfonamide (CSAS) is used in the synthesis of xipamide, a diuretic compound [46, 47]. It has been shown that 4-chloric salicylic acid-

5-sulfonamide and its derivatives are compounds that have diuretic properties [48, 49]. The current study focuses on the ability of 4-chloric salicylic acid-5-sulfonamide to form multicomponent crystals, such as hydrates, cocrystals, and polymorphs.

The crystalline structures of two different hydrates (2-hydrate and 3-hydrate in Fig. 5.1b), a cocrystal with benzoic acid, (4-cocrystal in Fig. 5.1c), a multicomponent structure with 4,4'-bipyridine and 1,4-dioxane (5-multicomp from Fig. 5.1d) and four polymorphs (Polymorph 1, 2, 3, 4 in Fig. 5.1a) were determined by X-ray single crystals diffraction. [50, 51]. The newly formed materials were also characterized by X-ray powder diffraction, FTIR spectroscopy and lattice energies were analyzed. The four polymorphs were also investigated by DSC thermal analysis and characterized in terms of intermolecular interactions by Hirshfeld surfaces.

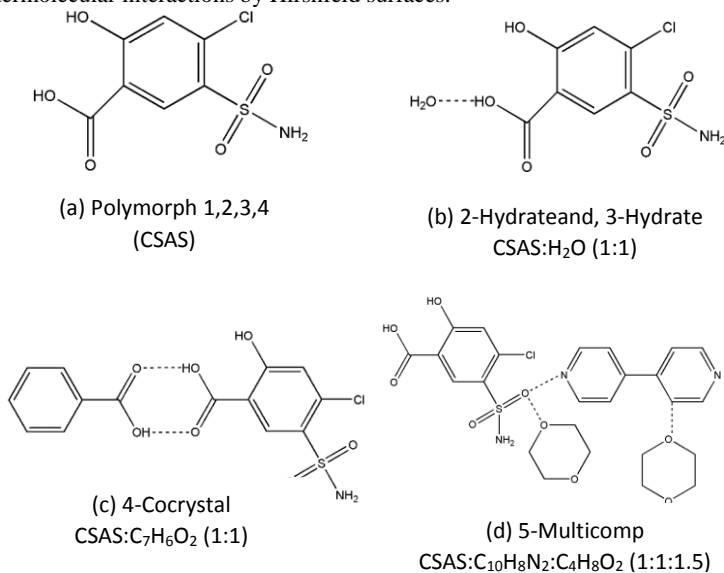


Figure 5.1: Chemical schemes of investigated solid forms

The above-mentioned solid forms were obtained by several crystallization processes: parallel crystallization with different temperature regimes and solvent mixtures, grinding followed by recrystallization by slow evaporation. Hydrates were obtained in a solution of methanol (2-hydrate) and acetone solution (3-hydrate). In the case of cocrystals, the initial compound was mixed with benzoic acid and 4,4'-bipyridine as coformer in a 1:1 stoichiometric ratio. The solvent used was methanol for 4-cocrystal and 1,4-dioxane for 5-multicomp. Also, the 4-cocrystal form was successfully obtained by mechanochemistry using ball grinding technique, and a few drops of methanol as activating agent, at a frequency of 27 Hz for 60 minutes. Suitable single crystals of

polymorph 1, which is the start compound, were obtained in methanol, polymorph 2 in ethyl acetate, polymorph 3 in 2-butanone and polymorph 4 in 5-methyl-2-hexanone.

### Crystal structures analysis

The most important structural results obtained from the crystal structures of the eight solid forms are presented in table 5.1.

Table 5.1: Crystal structure data for the eight solid forms studied.

Compound	Polymorph 1	Polymorph 2	Polymorph 3	Polymorph 4
Empirical formula	C <sub>7</sub> H <sub>6</sub> ClNO <sub>5</sub> S			
Molecular weight	251.64	251.64	251.64	251.64
Temperature/K	293	293	293	293
Crystal system	monoclinic	tetragonal	monoclinic	monoclinic
Space group	P2 <sub>1</sub> /c	P4/n	P2 <sub>1</sub> /c	P2 <sub>1</sub> /c
a/Å	9.53	19.87	5.48	9.27
b/Å	6.08	19.87	9.68	7.47
c/Å	16.11	5.33	17.75	17.38
α/°	90	90	90	90
β/°	95.43	90	94.90	130.49
γ/°	90	90	90	90
Volume/Å <sup>3</sup>	929	2108	939	916
Z	4	8	4	4
ρ <sub>calc</sub> /cm <sup>3</sup>	1.797	1.586	1.780	1.824

Table 5.1 (continued): Crystal structure data for the eight solid forms studied.

Compound	2-hydrate	3-hydrate	4-cocrystal	5-multicomp
Empirical formula	$C_7H_8ClNO_6S$	$C_7H_8ClNO_6S$	$C_{14}H_{12}ClNO_7S$	$C_{21}H_{22}ClN_3O_7S$
Molecular weight	269.65	269.65	373.76	495.92
Temperature/K	293	293	293	105
Crystal system	monoclinic	orthorhombic	monoclinic	monoclinic
Space group	$P2_1/c$	$Pbca$	$P2_1/n$	$P2_1/n$
$a/\text{\AA}$	9.23	11.81	6.74	9.71
$b/\text{\AA}$	8.07	6.83	31.43	17.40
$c/\text{\AA}$	14.91	25.68	7.47	12.77
$\alpha/^\circ$	90	90	90	90
$\beta/^\circ$	107.45	90	91.11	93.41
$\gamma/^\circ$	90	90	90	90
Volume/ $\text{\AA}^3$	1061	2074	1582	2157
Z	4	8	4	4
$\rho_{\text{calc}}/\text{g/cm}^3$	1.688	1.727	1.568	1.527

The purity of the solid forms obtained and the fact that the crystal structures determined from single crystals are the same as the crystal structures of the powders from which they came was made by comparing the experimental X-ray patterns with those simulated based on CIF files from single crystals. We present (Fig. 5.2) this comparison only for polymorph 1 and the cocrystal with benzoic acid (4-cocrystal).

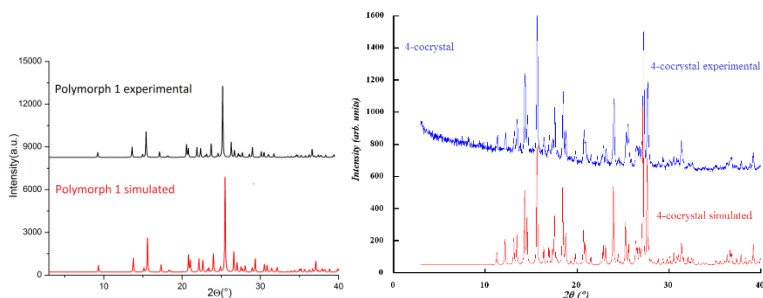


Figure 5.2: Comparison between experimental and simulated patterns: polymorph 1 and 4-cocrystal

All these polymorphs form supramolecular assemblies through the N-H...O and O-H...O hydrogen bonds. Polymorphs 2,3 and 4 form  $R^2_2(8)$  synthons types through mutual O-H...O carboxyl-carboxyl bonds. The centroids of these synthons are placed in special positions such as on the faces  $(0, \frac{1}{2}, \frac{1}{2})$ , the center of the cell  $(\frac{1}{2}, \frac{1}{2}, \frac{1}{2})$ , on the edges  $(0, 0, \frac{1}{2})$  and on the corners  $(0 0 0)$ . We exemplify the description of the crystal structure for polymorph 3.

The crystal structure of polymorph 3 can be described by a structural unit consisting of two molecules connected by reciprocal O1-H1...O2 carboxyl-carboxyl hydrogen bonds forming a  $R^2_2(8)$  ring motif. The two constituent molecules of the unit are linked by the inversion operation, with the centroid at  $(0 0 0)$ . In the elementary cell there are two such blocks linked by the symmetry operation  $2_1/c$ . One unit has its centroid located at  $(0, 0, 0)$  and the second at  $(0, \frac{1}{2}, \frac{1}{2})$  (Fig. 5.3). The two supramolecular assemblies are connected by the N1-H1A...O3 hydrogen bond between the N1 nitrogen of the amide and the hydroxyl of the phenyl ring.

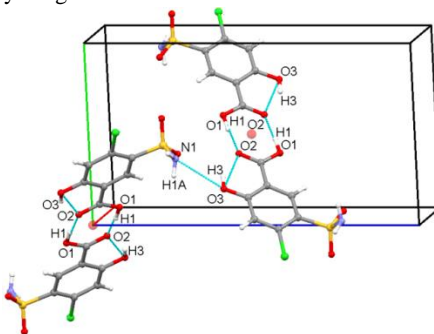


Figure 5.3:  $R^2_2(8)$  ring motifs placed in special positions in polymorph 3

It is interesting to note that polymorphs 1, 2 and 4 are enantiomers of the same type, while for polymorph 3, the amide group is the mirror image of polymorphs 1, 2 and 4. Thus, by recrystallization in 2-butanone (polymorph 3), a single enantiomer was separated from the racemic molecules (Fig. 5.4).

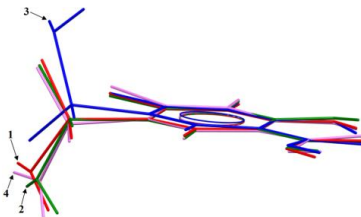


Figure 5.4: Molecular overlap: polymorph 1-red, polymorph 2-green, polymorph 3-blue, polymorph 4-purple

In multi-component crystals, supramolecular assemblies are formed via O-H...O and N-H...O hydrogen bonds. The centroids of these structural units are placed in special positions. For example the solid 2-hydrate form has the positions  $(\frac{1}{2}, \frac{1}{2}, \frac{1}{2})$  and  $(\frac{1}{2}, 0, 0)$ , the solid 3-hydrate form  $(\frac{1}{2}, \frac{1}{2}, \frac{1}{2})$ , the benzoic acid cocrystal in  $(\frac{1}{2}, \frac{1}{2}, 0)$  and  $(\frac{1}{2}, \frac{1}{2}, \frac{1}{2})$  and the cocrystal-solvate in the positions  $(\frac{1}{2}, \frac{1}{2}, \frac{1}{2})$ , on the *boc* face  $(0, \frac{1}{2}, \frac{1}{2})$ , and on the *oa*-axis  $(\frac{1}{2}, 0, 0)$ . We exemplify the description of the crystal structure for the compound 4-crystal.

The compound 4-crystal has a stoichiometric ratio of 1:1 CSAS:benzoic acid. The basic structural unit consists of a CSAS molecule and a benzoic acid molecule linked by reciprocal O1-H1...O6 and O7-H7A...O2carboxyl-carboxyl hydrogen bonds. This structural unit consisting of CSAS and benzoic acid is approximately planar, except for oxygen O5 and nitrogen N1 in the sulfonamide group, having RMSD=0.06. This structural unit exhibits  $\pi$ ... $\pi$  stacking interactions with another unit identical and parallel to the first, the distance between the two being 3.50 Å and forming a supramolecular assembly centered at the special position  $(\frac{1}{2}, \frac{1}{2}, \frac{1}{2})$  of the space group P2<sub>1</sub>/n (Fig. 5.5). The neighbouring supramolecular assemblies are centred at the  $(1, 0, \frac{1}{2})$  and  $(0, 1, \frac{1}{2})$  positions and are connected to each other by N1-H1A...O4 hydrogen bonds.

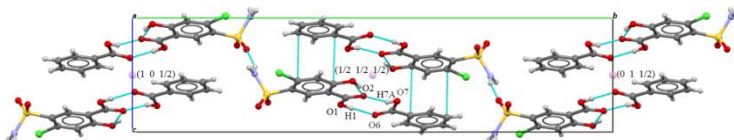


Figure 5.5: Elementary cell packing scheme of compound 4-crystal

A remarkable feature is that, 2-hydrate and 5-multicomp compounds are enantiomers of the same type, whereas, 3-hydrate and 4-crystal are enantiomers of different types (Fig. 5.6). The 3-hydrate and 4-crystal compounds are the mirror image of the 2-hydrate and 5-multicomp compounds. Through the recrystallisation process it is possible to separate the two types of enantiomers from the racemic molecules.

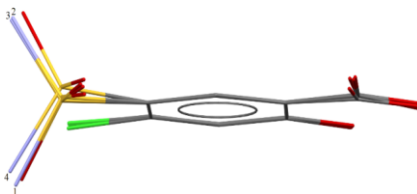


Figure 5.6: Molecular superposition of CSAS molecules, other structural components being omitted

### Calculation of lattice energies

The partitioned lattice energies detailed in Table 5.2 show that dispersion energies are the dominant components in all crystal structures. The starting material (polymorph 1) and the other polymorphs show considerably higher total and partitioned lattice energies (in absolute value) compared to the multi-component structures.

Table 5.2: Lattice energies

$E_{\text{coul}}$ : Coulombic term;  $E_{\text{pol}}$ : polarization;  $E_{\text{disp}}$ : dispersion;  $E_{\text{att}}$ : attraction;  $E_{\text{rep}}$ : repulsion;  $E_{\text{latt}}$ : CLP crystal lattice energy

Structure	$E_{\text{coul}}$ (kJ/mol)	$E_{\text{pol}}$ (kJ/mol)	$E_{\text{disp}}$ (kJ/mol)	$E_{\text{att}}$ (kJ/mol)	$E_{\text{rep}}$ (kJ/mol)	$E_{\text{latt}}$ (kJ/mol)
Polymorph 1	-19.9	-74.8	-137.1	-231.8	79.9	-151.9
Polymorph 2	-24.0	-69.4	-122.5	-215.9	69.6	-146.3
Polymorph 3	-26.5	-73.7	-132.1	-232.3	63.3	-169.0
Polymorph 4	-22.2	-76.3	-138.6	-237.1	71.2	-166.0
2-hydrate	-19.5	-47.0	-78.5	-145.0	51.8	-93.3
3-hydrate	-19.0	-46.7	-79.9	-145.6	47.5	-98.2
4-cocrystal	-18.8	-43.8	-103.0	-165.6	53.7	-111.9
5-multicomp	-15.0	-12.2	-51.1	-78.3	23.0	-55.3

### DSC and FTIR analysis

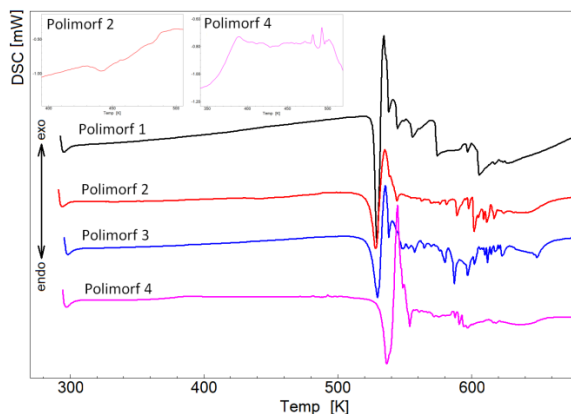


Figure 5.7: DSC curves of polymorphs 1, 2, 3 and 4

The DSC calorimetric analysis of the four polymorphs shows that polymorphs 1 and 3 are pure, no residual solvent can be observed, they show a single endothermic

melting signal followed by decomposition (Fig. 5.7). In the case of polymorph 2 a solid-solid phase transition was observed, after which polymorph 2 becomes polymorph 1. The DSC curve of polymorph 4 reveals three low-intensity exothermic signals between 360-500 K, possible due to residual solvent removal (boiling point of 5-methyl-2-hexanone is 417 K).

By IR analysis, specific bands were assigned to functional groups and at the same time the formation of new solid forms proved by X-ray diffraction was confirmed.

Hirshfeld and fingerprint analysis shows that O-H...O hydrogen bonds play the most important role in the crystal stability of the polymorphs, which can be seen from the high percentages of O...H/H...O contacts. On the other hand, polymorph 2 has much larger  $d_i$  and  $d_e$  distances than the rest of the polymorphs (these values exceed 2.8 Å), resulting in a lower packing efficiency, a result also obtained from the evaluation of the CLP lattice energies.

## 6. Copper complexes with sulphonamides

The continuous demand for new anti-cancer drugs stimulates chemotherapeutic research based on the use of less toxic metal compounds with better antiproliferative activity against tumors [52], thus a large number of chemicals are known to have biocatalytic activity in vitro, stimulating different enzymatic processes. Among these chemicals, copper-coordinated compounds exhibit dismutase activity or nuclease activity depending on the type of ligand present. Although many studies have been done, metal-containing drugs are rare.

We have dealt with the following copper complexes with sulphonamides:

**L1:** 4-Methyl-N-(5-(4-methylphenyl)-1,3,4-thiadiazol-2-yl)benzenesulfonamide (C<sub>16</sub> H<sub>15</sub> N<sub>3</sub> O<sub>2</sub> S<sub>2</sub>)

**C1:** Cu (II) [Cu(L)<sub>2</sub>(Py)<sub>2</sub>(H<sub>2</sub>O)] (HL = 4-Methyl-N-(5-(4-methylphenyl)-1,3,4-thiadiazol-2-yl)benzenesulfonamide) (C<sub>42</sub> H<sub>41</sub> Cu N<sub>8</sub> O<sub>5</sub> S<sub>4</sub>)

**C2:** [Cu(L)<sub>2</sub>(py)<sub>2</sub>] (HL= N-(5-(4-methoxyphenyl)-[1,3,4]-thiadiazole-2-yl)-toluenesulfonamide)

**C3:** [Cu(L)<sub>2</sub>(py)-2(H<sub>2</sub>O)] (HL= N-(5-(4-methylphenyl)-[1,3,4]-thiadiazole-2-yl)-benzenesulfonamide) (C<sub>40</sub> H<sub>35</sub> Cu N<sub>8</sub> O<sub>5</sub> S<sub>4</sub>)

**C4:** bis(5-(4-methoxyphenyl)-2-((2-naphthylsulfonyl)imino)-1,3,4-thiadiazol-3(2H)-yl)-bis(pyridine)-copper(II) (C<sub>48</sub> H<sub>38</sub> Cu N<sub>8</sub> O<sub>6</sub> S<sub>4</sub>)

**C5:** (5-(4-methoxyphenyl)-2-((2-naphthylsulfonyl)imino)-1,3,4-thiadiazol-3(2H)-yl)- bis(1,10-phenanthroline)-copper(ii) 5-(4-methoxyphenyl)-2-((naphthalen-2-yl)sulfonyl)imino)-2H-1,3,4-thiadiazol-3-ide methanol solvate (C<sub>43</sub> H<sub>30</sub> Cu N<sub>7</sub> O<sub>3</sub> S<sub>2</sub><sup>+</sup>, C<sub>19</sub> H<sub>14</sub> N<sub>3</sub> O<sub>3</sub> S<sub>2</sub><sup>-</sup>, 1.25(C H<sub>4</sub> O)

**C6:** Cu(N-(5-(4-methylphenyl)-[1,3,4]-thiadiazole-2-yl)-toluenesulfonamidate)<sub>4</sub> ((CH<sub>3</sub>)<sub>2</sub>NH<sub>2</sub><sup>+</sup>)<sub>2</sub> (C<sub>68</sub>H<sub>72</sub>CuN<sub>14</sub>O<sub>8</sub>S<sub>8</sub>)

The crystal structures for L1 and the six complexes were determined by single crystal X-ray diffraction and the most important results are shown in Table 6.1.

Table 6.1. Most important crystallographic data

Structure	L1	C1	C2	C3
Empirical formula	$C_{16}H_{15}N_3O_2S_2$	$C_{42}H_{41}CuN_8O_5S_4$	$C_{22}H_{20}Cu_{0.5}N_2O_4S_2$	$C_{40}H_{35}CuN_8O_5S_4$
Molecular mass	345.44	929.63	472.29	899.32
Temperature/K	293	293	293	293
Crystal system	Triclinic	Monoclinic	Triclinic	Monoclinic
Space group	P-1	Cc	P-1	Cc
a/Å	6.56	15.09	7.91	15.09
b/Å	10.65	21.79	12.25	21.79
c/Å	13.53	13.13	12.77	13.13
$\alpha/^\circ$	67.59	90	112.06	90
$\beta/^\circ$	88.55	103.37	94.61	103.37
$\gamma/^\circ$	72.13	90	108.82	90
Volume/Å <sup>3</sup>	828	4205	1058	4205
Z	2	4	2	4
$\rho_{calc}mg/mm^3$	1.432	1.468	1.482	1.468

Structure	C4	C5	C6
Empirical formula	$C_{24}H_{19}Cu_{0.5}N_4O_3S_2$	$C_{43}H_{30}CuN_7O_3S_2 + C_{19}H_{14}N_3O_3S_2 \cdot 1.25(CH_4O)$	$C_{22}H_{20}Cu_{0.5}N_2O_4S_2$
Molecular mass	507.33	1256.47	472.29
Temperature/K	293	293	293
Crystal system	Monoclinic	Triclinic	Triclinic
Space group	P2 <sub>1</sub> /n	P-1	P-1
a/Å	12.72	14.44	7.91
b/Å	7.98	14.58	12.25
c/Å	22.11	15.30	12.77
$\alpha/^\circ$	90	94.04	112.06
$\beta/^\circ$	96.64	106.46	94.61
$\gamma/^\circ$	90	109.38	108.82
Volume/Å <sup>3</sup>	2231	2867	1058
Z	4	2	2
$\rho_{calc}mg/mm^3$	1.513	1.486	1.482

## Ligand L1 and complex C1

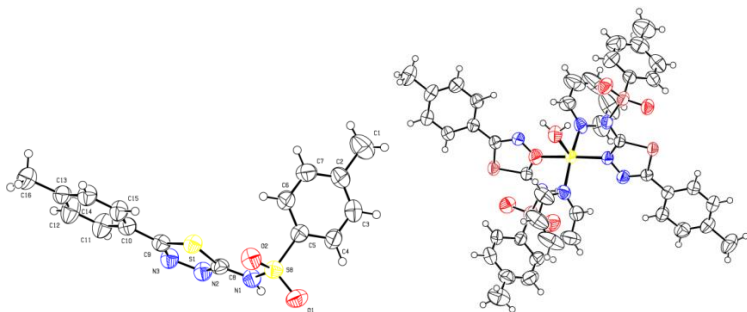


Figure 6.1: Ortep diagram of compound L1 (a) and complex C1 (b) with non-hydrogen atoms represented as thermal ellipsoids

In C1, the  $\text{Cu}^{2+}$  ion is five-coordinated, forming a  $\text{CuN}_4\text{O}$  chromophore. The ligand acts as a monodentate, coordinating the metal ion through a single N-thiadiazole atom. Molecules in the reaction medium (pyridine and water) are also involved in the coordination of the  $\text{Cu}^+$  ion. Complex I has a slightly distorted square pyramidal geometry [53].

## Complexes C2 and C3

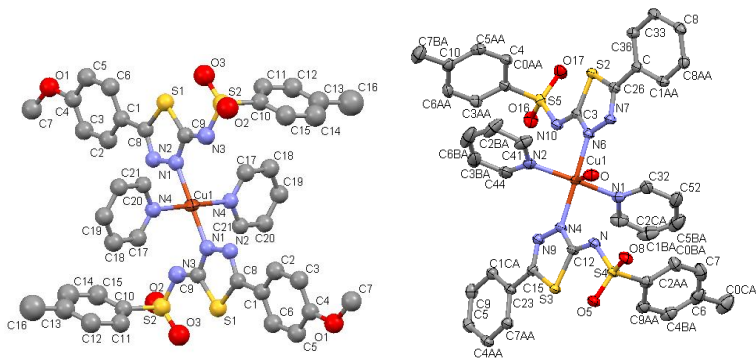


Figure 6.2: Molecular structure for complex C2 (a) and C3 (b)

The crystal structure for the C2 complex shows that the  $\text{Cu}(\text{II})$  ion is four coordinated and the chromophore type is  $\text{CuN}_4$ . The  $\text{Cu}(\text{II})$  ion is centrosymmetrically bound to two deprotonated ligands and two pyridine molecules in a square planar geometry. Each ligand coordinates the metal ion through a thiadiazole N atom, with average  $\text{Cu1-N1}$  bond distances  $1.961\text{\AA}$ . The crystal structure of the C2 complex consists

of monomer units linked by stacking interactions between the aromatic rings of the pyridine molecules (average ring spacing being 3.731 Å) [54].

In the C3 complex, the coordination geometry of the metal ion is slightly deformed from the square-pyramidal geometry. Intermolecular  $\pi$ - $\pi$  interactions between pyridine and the benzene ring in the same molecule and pyridine molecules and the toluene ring in adjacent molecules contribute to the stabilization of the C3 complex. The C3 complex is stabilized by strong and weak hydrogen bonds involving the hydrogens of the water molecule and N<sub>sulfonamide</sub>, N<sub>thiadiazole</sub> and the hydrogen atoms of the benzene ring with atoms corresponding to the sulfonamide group.

### Complexes C4 and C5

Molecular structures and crystallographic numbering schemes are illustrated in Fig. 6.3a for the C4 complex respectively Fig. 6.3b for complex C5.

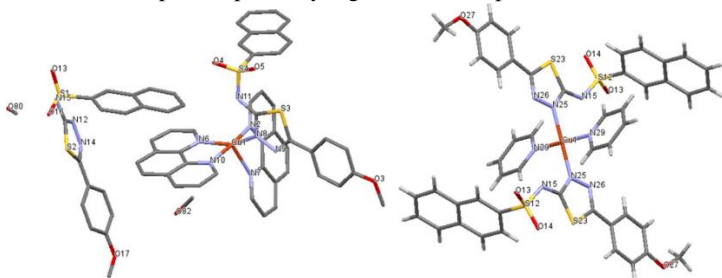


Figure 6.3: Molecular structure of C4 complex (a) and C5 complex (b)

The crystal structure of the complex C4 shows that the copper atom is four times coordinated and the chromophore type is CuN<sub>4</sub>. The copper atom is centrosymmetrically bonded to two deprotonated L ligands, plus two pyridine ligands in a square planar form. Each L ligand coordinates to the metal through the N atom of the thiadiazole, with Cu1-N1 spacings of 1.977 Å [55].

The C5 complex is five coordinated in a CuN<sub>5</sub> chromophore. The coordination geometry of the central metal is in the form of a slightly distorted square pyramid. Equatorial bonds are shorter, ranging from 2,009 Å to 2,065 Å. The N<sub>4</sub> equatorial plane consists of one nitrogen atom from the deprotonated sulfonamide (N<sub>thiadiazole</sub>) and two nitrogen atoms from the 1,10-phenanthroline group (N<sub>fen</sub>).

## Complex C6

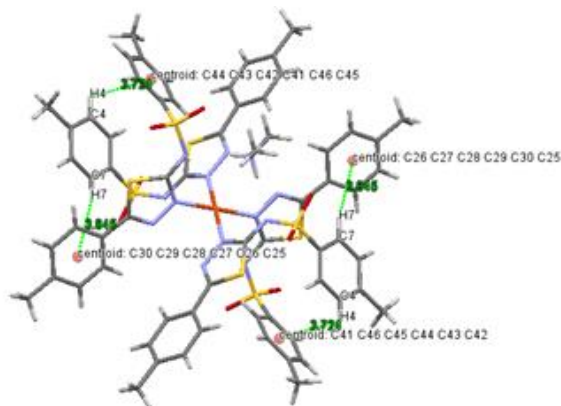


Figure 6.4: Molecular structure of the C6 complex

The molecular structure and crystallographic numbering scheme of the C6 complex is illustrated in Fig. 6.4. The crystal structure of the complex contains a  $\text{CuN}_4$  entity in a square plane geometry. In this complex, the  $\text{Cu(II)}$  ion is coordinated by four ligand molecules. Each ligand acts as a monodentate and coordinates the metal ion through an  $\text{N}_{\text{thiadiazole}}$  atom of the thiadiazole ring [56].

### General conclusions

1. Single crystals of five boldenone-based compounds were obtained by recrystallization in solutions and their crystal structure was determined: boldenone base, two polymorphs of boldenone acetate, boldenone propionate and boldenone cypionate. Boldenone base and boldenone propionate crystallize in the monoclinic system,  $\text{P2}_1$  space group while the polymorphs of boldenone acetate and boldenone cypionate crystallize in the orthorhombic system having space group  $\text{P2}_1\text{2}_1\text{2}_1$ . The supramolecular network of boldenone base is characterized by infinite  $\text{O-H}\dots\text{O}$  chains of hydrogen bonds along the  $oc$  axis and  $\text{C-H}\dots\text{O}$  and  $\text{C-H}\dots\text{H-C}$  interactions between the chains, while the lattices of Ba, Ba1, Bp, Bc are aggregated by a combination of  $\text{C-H}\dots\text{O}$  and  $\text{C-H}\dots\text{H-C}$  interactions. These intermolecular contacts were visualized by means of Hirshfeld surfaces and the calculation of the lattice energies shows that dispersive interactions predominate the structures. The molecular conformation of six and five membered rings of each compound was determined.

2. Single crystals were obtained for two trenbolone esters, and their crystal structure was solved by single crystal X-ray diffraction: trenbolone acetate and hexahydrobenzylcarbonate crystallize in the monoclinic crystallographic system, space

group  $P2_1$ . Trenbolone acetate has a rare structure in the sense it has four molecules in the asymmetric unit whereas trenbolone hexahydrobenzylcarbonate contains only one molecule in the asymmetric unit. The third structure, namely enanthate trenbolone, since no suitable single crystals could be obtained, was resolved by powder diffraction and belongs to the space group  $P2_1$  with two molecules in the asymmetric unit. The crystal structure of the unesterified trenbolone form is characterized by strong O-H...O hydrogen bonds arranged in chains along the *oz*-axis, while the supramolecular arrangements in the esterified forms, Tren Ac, Tren Hex, Tren En are stabilized by C-H...O and C-H... $\pi$  interactions. Based on the asymmetry parameters, it is shown that the steroid skeleton rings are found in various envelope conformations, but strongly distorted except for Tren Hex. Analysis of Hirshfeld surfaces, fingerprint diagrams and CLP lattice energies shows that lattice stability is based on dispersion interactions.

3. Two polymorphs of drostanolon propionate were grown by recrystallization and their crystal structures were determined by single crystal X-ray diffraction, both belonging to the monoclinic system. The one obtained from ethanol solution has the space group  $P2_1$  and the one from acetone the rare space group  $I2$ . Since no single crystals could be grown for the starting compound, its crystal structure was determined from powders resulting in the orthorhombic space group  $P2_12_12_1$ . From the fingerprint, Hirshfeld diagrams and lattice energy analysis it appears that the most important contributions to the lattice energies are made by the H...H, O...H/H...O contacts. The six-membered rings adopt a chair conformation while the five-membered rings have an envelope conformation.

4. Single crystals of the compounds ostarine and andarine were grown and their crystal structure was determined by single crystal X-ray diffraction resulting in ostarine having a monoclinic crystallographic system, space group  $P2_1$  and andarine being tetragonal with the rare  $P4_22_12$  space group. A polymorph of ostarine was obtained by heating the starting compound at 125°C. This phase transformation was evidenced by DTA thermal analysis. The formation of this polymorph was confirmed by X-ray powder diffraction and the crystal structure of this polymorph was also determined and the space group was determined to be  $P2_1$ . IR analysis showed that this compound is a polymorph and not another solid form (hydrate, solvate). The supramolecular assemblies in the crystals are formed by N-H...O and O-H...O hydrogen bonds. An interesting structural feature for ostarine is that it exhibits significantly sized tunnel-shaped voids. By CLP analysis it appears that the newly formed polymorph is less stable.

5. Sodium (2-carbamoylphenoxy) acetate salt belongs to the space group  $P-1$  of the triclinic system,  $Z=2$ . The asymmetric part of the unit cell consists of four (2-carbamoylphenoxy) acetate molecules. Three  $\text{Na}^+$  ions are surrounded by six O atoms and one  $\text{Na}^+$  ion is surrounded by five O atoms. The average distance  $\text{Na}1^+\dots\text{O}$  and  $\text{Na}2^+\dots\text{O}$  is 2.47 Å, while  $\text{Na}3^+\dots\text{O}$  is 2.43 Å and  $\text{Na}4^+\dots\text{O}$  is 2.49 Å. Supramolecular

packing of the four (2-carbamoylphenoxy) acetate molecules is achieved by hydrogen bonds and a variety of intermolecular interactions forming  $R^2_2(18)$  and  $R^2_2(8)$  synthons. It has been established by IR, Raman spectroscopy and X-ray diffraction that following a treatment with hydrochloric acid, the sodium is removed from the crystal structure and results a new compound.

6. Eight solid forms of the diuretic compound 4-chloro salicylic acid-5-sulfonamide, of which four multicomponent structures: two hydrates, one cocrystal with benzoic acid and one cocrystal-solvate with 4,4'-bipyridine plus 1,4-dioxane and four polymorphs were obtained by parallel recrystallization. Crystal structures were determined by single crystal X-ray diffraction technique and in addition, structural characterization was performed by X-ray powder diffraction on and FT-IR. The total crystal lattice energy, was calculated and it was observed that multicomponent structures are less stable compared to polymorphs. For the two hydrates, the molecular assemblies are connected by N-H...O and O-H...O hydrogen bonds. The benzoic acid cocrystal has the molecule bonded to the benzoic acid in a 1:1 stoichiometric manner via O-H...O carboxyl-carboxyl hydrogen bonds, forming an  $R^2_2(8)$  homosynthons. The multicomponent cocrystal-solvent system is stabilized by a combination of C-H...O and N-H...O hydrogen bonds between the solvent, 4,4' bipyridine and the starting compound.

In the case of polymorphs, the thermal behavior was further investigated by DSC analysis. The supramolecular assemblies in the case of polymorphs are stabilized by a combination of O-H...O, C-H...O and N-H...O hydrogen bonds. By means of strong carboxyl-carboxyl O-H...O hydrogen bonds, three of the polymorphs form centrosymmetric dimers containing  $R^2_2(8)$  motifs. Hirshfeld surface analysis was used to reveal additional details about intermolecular interactions in polymorphs.

7. A ligand and six copper complexes with sulfonamides which have antiproliferative activity against cancer were synthesized and recrystallized. Their crystal structures were determined by single crystal X-ray diffraction. The ligand crystallizes in the triclinic system, P-1 space group with one molecule in the asymmetric unit. Four of the complexes also belong to the triclinic system, space group P-1 with two molecules in the elementary cell; two of the complexes crystallize in the monoclinic system, space group Cc with four molecules in the elementary cell and one of the complexes belongs to space group  $P2_1/n$  also having four molecules in the unit cell. In three of the complexes the copper  $Cu^{2+}$  ion has coordination four and for other three complexes the copper coordination is five.

In total, crystal structures for 30 biologically active compounds/solid forms were determined and characterized by diffractometric, spectroscopic, thermal and computational methods.

## List of publications in ISI journals

**On the subject of the thesis: 12 papers, of which 8 I am first author or corresponding author:**

1. A. C. Hangan, **A. Turza**, R. L. Stan, R. Stefan, L. S. Oprean, Synthesis, crystal structure, properties, and nuclease activity of a new Cu(II) complex [Cu(L)(2)(Py)(2)(H<sub>2</sub>O)] (HL = N-(5-(4-methylphenyl)-[1,3,4]-thiadiazole-2-yl)toluenesulfonamide), *Russ. J. Coord. Chem.* 41, 2015, 395-404.
2. A.C. Hangan, **A. Turza**, R.L. Stan, B. Sevastre; E. Pall, S. Cetean, L.S. Oprean. Synthesis, crystal structure and characterization of new biologically active Cu(II) complexes with ligand derived from N-substituted sulfonamide, *J. Chem. Sci.* 128, 2016, 815-824.
3. A.C. Hangan, R. L. Stan, **A. Turza**, L. S. Oprean, E. Pall, S. Gheorghe-Cetean, B. Sevastre, Synthesis, crystal structures, characterization and antitumor activities of two copper(II) complexes of a sulfonamide ligand, *Transit. Met. Chem.* 42, 2017, 153-164.
4. A.C. Hangan; **A. Turza**, R.L. Stan, L.S. Oprean. Synthesis, Crystal Structures and Characterization of a New Antitumor Cu(II) Complex with N-sulfonamide Ligand, *Rev. Chim.* 69, 2019, 1407-1410.
5. G. Borodi, **A. Turza**, A. Bende Exploring the Polymorphism of Drostanolone Propionate, *MOLECULES*, 26, 2020, 1436.
6. **A. Turza**, A. Aurel, M. Muresan-Pop, L. Zarbo, G. Borodi Crystal and molecular structure of ostarine and andarine *J. Mol. Struct.* 1199, 2020, 126973.
7. **A. Turza**, M.O. Miclaus, A. Pop, G. Borodi, Crystal and molecular structures of boldenone and four boldenone steroid esters, *Z. Kristallogr. Cryst. Mater.* 234, 2019, 671-683.
8. G. Borodi, **A. Turza**, P. A. Camarasan, A. Ulici Structural studies of Trenbolone, Trenbolone Acetate, Hexahydrobenzylcarbonate and Enanthate esters, *J. Mol. Struct.* 1212, 2020, 128127,
9. **A. Turza**, G. Borodi, M.O. Miclaus, I. Kacso, Structural studies of the diuretic compound 4-Chloro Salicylic Acid-5-Sulfonamide, *J. Mol. Struct.* 1212, 2020, 128154.
10. **A. Turza**, A. M. R. Gherman, V. Chis, C. B. Grosan, G. Borodi, Structural, spectroscopic and theoretical studies of sodium (2-carbamoylphenoxy) acetate salt, *J. Mol. Struct.* 1200, 2020, 127016.
11. G. Borodi, **A. Turza**, O. Onija, A. Bende, Succinic, fumaric, adipic and oxalic acid cocrystals of promethazine hydrochloride, *Acta Cryst. C* 75, 2019.
12. **Turza Alexandru**, Miclaus O. Maria, Zarbo Liviu, David Maria, Kacso Irina, Borodi Gheorghe, New solid forms of the diuretic compound 4-Chloro Salicylic Acid-5-Sulfonamide, *J. Mol. Struct.* accepted.

### **Other ISI papers:**

1. M. Coros, F. Pogacean, **A. Turza**, M. Dan, C. Berghian-Grosan, I. O. Pana, S. Pruneanu Green synthesis, characterization and potential application of reduced graphene oxide, *Physica E Low Dimens. Syst. Nanostruct.* 119, 2020, 113971.

2. M. Coros, C. Socaci, S. Pruneanu, F. Pogacean, M. C. Rosu, **A. Turza**, L. Magerusan, Thermally reduced graphene oxide as green and easily available adsorbent for Sunset yellow decontamination, *Environ. Res.* 182, 2020, 109047.
3. C.M. Muntean, N. E. Dima, M. Coros, N. Tosa, **A. Turza**, M. Dan, Graphene/silver nanoparticles-based surface-enhanced Raman spectroscopy detection platforms: Application in the study of DNA molecules at low pH, *J. Raman Spectrosc.* 50, 2019, 1849-1860.
4. L. Magerusan, C. Socaci, F. Pogacean, M. C. Rosu, A. R. Biris, M. Coros, **A. Turza**, V. Floare-Avram, G. Katona, S. Pruneanu, Enhancement of peroxidase-like activity of N-doped graphene assembled with iron-tetrapyrridylporphyrin, *RSC Adv.* 6, 2016, 79497-79506.
5. M. C. Rosu, M. Coros, F. Pogacean, L. Magerusan, C. Socaci, **A. Turza**, S. Pruneanu, Azo dyes degradation using TiO<sub>2</sub>-Pt/graphene oxide and TiO<sub>2</sub>-Pt/reduced graphene oxide photocatalysts under UV and natural sunlight irradiation, *Solid State Sci.* 70, 2017, 13-20.
6. F. Pogacean, M. Coros, L. Magerusan, V. Mirel, **A. Turza**, G. Katona, R. I. Stefan-van Staden, S. Pruneanu, Exfoliation of graphite rods via pulses of current for graphene synthesis: Sensitive detection of 8-hydroxy-2'-deoxyguanosine, *Talanta*, 196, 2019, 182-190.
7. F. Pogacean, M. Stefan, D. Toloman, A. Popa, C. Leostean, **A. Turza**, M. Coros, O. Pana, S. Pruneanu, Photocatalytic and Electrocatalytic Properties of NGr-ZnO Hybrid Materials, *Nanomaterials*, 10, 2020, 1473.
8. L. Chirila, D. V. Cosma, A. Urda, A. S. Porav, **A. Turza**, D. Timpu, A. O. Mateescu, UV light-shielding properties of TiO<sub>2</sub>-based materials coated flax samples, *JOAM*, 22, 2020, 62-66.
9. M. C. Rosu, E. Pall, C. Socaci, L. Magerusan, F. Pogacean, M. Coros, **A. Turza**, S. Pruneanu, Cytotoxicity of methylcellulose-based films containing graphenes and curcumin on human lung fibroblasts, *Process Biochem.* 52, 2020, 243-249.
10. B. Stoean, D. Rugina, M. Focsan, A.M. Craciun, M. Nistor, T. Lovasz, **A. Turza**, I.D. Porumb, E. Gal, C. Cristea, L.S. Dumitrescu, S. Astilean, L.I. Gaina, Novel (Phenothiazinyl)Vinyl-Pyridinium Dyes and Their Potential Applications as Cellular Staining Agents, *IJMS*, 22, 2021.

## SELECTIVE REFERENCES

- [1] CrysAlis PRO 1.171.38.46, Rigaku Oxford Diffraction, 2015.
- [2] O.V. Dolomanov, L.J. Bourhis, R.J. Gildea, J.A.K. Howard, H. Puschmann, *J. Appl. Cryst.* 42, 2009, 339-341.
- [3] G.M. Sheldrick, (1997) SHELXS97 and SHELXL97. Program for Crystal Structure Solution and Refinement. University of Göttingen, Göttingen.
- [4] G.M. Sheldrick, *Acta Cryst.* A64, 2008, 112-122.

- [5] G.M. Sheldrick, *Acta Cryst.* A71, 2015, 3-8.
- [6] L.J. Bourhis, O.V. Dolomanov, R.J. Gildea, J.A.K. Howard, H. Puschmann, *Acta Cryst.* A71, 2015, 59-75.
- [7] G.M. Sheldrick, *Acta Cryst.* C71, 2015, 3-8
- [8] A. Meden, *Croat. Chem. Acta* 71, 1998, 615–633.
- [9] Dassault Systèmes BIOVIA, (2014). [Materials Studio], [v8.0.0.843], San Diego: Dassault Systèmes.
- [10] P-E. Werner, L. Eriksson, M. Westdahl, *J Appl. Cryst.* 18, 1985, 367–370.
- [11] A. Boultif, D. Louer, *J. Appl. Cryst.* 37, 2004 724-731.
- [12] M.A. Neumann, *J. Appl. Cryst.* 36, 2003, 356-365.
- [13] V. Favre-Nicolin, R. Černý, FOX, *J. Appl. Crystallogr.* 35, 2002, 734–743.
- [14] G.E. Engel, S. Wilke, O. König, K.D.M. Harris, F.J.J Leusen, *J. Appl. Crystallogr.* 32, 1999, 1169–1179.
- [15] G. Caglioti, A. Paoletti, F.P. Ricci, *Nucl. Instrum.* 3, 1958, 223-228.
- [16] Mark A. Spackman, Patrick G. Byrom, *Chemical Physics Letters*, 267, 1997, 215-220.
- [17] J.J. McKinnon, M.A. Spackman, A.S. Mitchell, *Acta Cryst.* B60, 2004, 627-668.
- [18] Joshua J. McKinnon, Mark A. Spackman, Anthony S. Mitchell, *Acta Cryst.* B60, 2004, 627-668.
- [19] J.J. McKinnon, D. Jayatilaka, M.A. Spackman, *Chem. Commun.* 37, 2007, 3814-3816.
- [20] A. Gavezzotti, *New J. Chem.* 35, 2011, 1360–1368.
- [21] J.F. Griffin, W.L. Duax, C.M. Weeks, *Atlas of Steroid Structure*, 2nd ed, IFI/PLENUM, New York-Washington-London, 1984.
- [22] A.T. Kicman, *Br. J. Pharmacol.* 154, 2008, 502–521.
- [23] P.C.A Kam, M. Yarrow, *Anaesthesia.* 60, 2005, 685–92.
- [24] A. Vermeulen, *Acta Clin. Belg.* 30, 1975, 48–55.
- [25] Elks, J.; Ganellin, C.R. *The Dictionary of Drugs: Chemical Data: Chemical Data, Structures and Bibliographies*, first ed.; Springer: Easton, ME, US, 1990, p. 652.
- [26] *Index Nominum 2000*, International Drug Directory Amer Pharmacists Assn, 17th ed., Swiss Pharmaceutical Society, 2000.
- [27] W. Llewellyn, *Anabolics*, 10th ed., Molecular Nutrition Llc., Jupiter, 2011.
- [28] **A. Turza**, M. O. Miclaus, A. Pop, G. Borodi, *Z. Kristallogr. Cryst. Mater.* 234, 2019, 671-683.

- [29] V.J. Dalbo, M.D. Roberts, C.B. Mobley, C. Ballmann, W.C. Kephart, C.D. Fox, V.A. Santucci, C.F. Conover, L.A. Beggs, A. Balazs, F.J. Hoerr, J.F. Yarrow, S.E. Borst, D.T. Beck, *Andrologia*, 49, 2016, 1-11.
- [30] G. Borodi, **A. Turza**, P.A. Camarasan, A. Ulici, *J. Mol. Struct.*, 1212, 2020.
- [31] C.R. Groom, I.J. Bruno, M.P. Lightfoot, S.C. Ward, *Acta Cryst. B*72, 2016, 171-179.
- [32] P. Grochulski, Z. Wawrzak, *J. Crystallogr. Spectrosc. Res.* 19, 1989, 577-587.
- [33] G. Borodi, **A. Turza**, A. Bende, *Molecules*, 25, (2020).
- [34] V.R. Hathwar, M. Sist, M.R.V. Jørgensen, A.H. Mamakhel, X. Wang, C.M. Hoffmann, K. Sugimoto, J. Overgaard, B.B. Iversen, *IUCrJ.* 2, 2015, 563-574.
- [35] C. Altona, H.J. Geise, C. Romers, *Tetrahedron*, 24, 1968, 13-32.
- [36] L. Mohler, C.E. Bohl, A. Jones, C.C. Coss, R. Narayanan, Y. He, D.J. Hwang, J.T. Dalton, D.D. Miller. *J. Med. Chem.* 52, 2009, 3597-3617.
- [37] R. Elancheran, V. L. Maruthanila, M. Ramanathan, S. Kabilan, R. Devi, A. Kunnumakara, J. Kotoky. *Med. Chem. Comm.* 6, 2015, 746-768.
- [38] **A. Turza**, A. Pop, M. M. Pop, L.Zarbo, G. Borodi, *J. Mol. Struct.* 1199, 2020, 126973.
- [39] MICROSIN products webpage, <http://microsin.ro/products.php> (accessed 02 August 2019)
- [40] B. Meurer-Witt, J. Biehl, Rapidly acting analgesic for treating acute, severe pain, comprises intravenously administered aqueous solution of o-carbamoyl-phenoxyacetic acid, DE Patent DE10032224A1, 2000
- [41] **A. Turza**, A. M. R. Gherman, V. Chis, C. B. Grosan, G. Borodi, *J. Mol. Struct.*, 1200, 2020, 127016.
- [42] G. Socrates, *Infrared and Raman Characteristic Group Frequencies*, third ed., Wiley-Interscience, John Wiley & Sons, Inc., Chichester, 2001
- [43] J. Bernstein, *Polymorphism in Molecular Crystals*, Oxford University Press, 2002.
- [44] S.R. Byrn, R.R. Pfeiffer, J.G. Stowell. *Solid-state chemistry of drugs*. Indiana: SSCI Inc 1999:10-15.
- [45] C.B. Aakeroy, D.J. Salmon. *Cryst. Eng. Comm.* 7, 2005, 439-448.
- [46] V. Alagarsamy, *Textbook of medicinal chemistry*, Volume 1, first ed., Elsevier India, 2009, pp 576.
- [47] FRG Pat. No. 1281428, 1969, Ref. Zh. Khim., No. 17N350P (1970).
- [48] W. Liebenow, F. Leuschner, *Arzneim.-Forsch.* 25, 1975, 240-244.
- [49] A.A. Lebedev, M.Yu. Bazhmina, V.A. Smirnov, *Pharm. Chem. J.* 21, 1987, 641-645.

- [50] **A. Turza**, G. Borodi, M. O. Miclaus, I. Kacso, *J. Mol. Struct.*, 1212, 2020, 128154.
- [51] **A. Turza**, M. O. Miclaus, L. Zarbo, M. David, I. Kacso, G. Borodi, New solid forms of the diuretic compound 4-Chloro Salicylic Acid-5-Sulfonamide, *J. Mol. Struct.*, accepted (2021)
- [52] J.L. Garcia-Giménez, M. González-Álvarez, M.J. Liu-González, *Inorg. Biochem.* 2009, 103, 923.
- [53] A.C. Hangan, **A. Turza**, R.L. Stan, R. Stefan, L.S. Oprean, *Russ. J. Coord. Chem.* 41, 2015, 395-404.
- [54] A.C. Hangan, **A. Turza**, R.L. Stan, B. Sevastre, E. Pall, S. Cetean, L.S. Oprean, *J. Chem. Sci.* 128, 2016, 815-824.
- [55] A.C. Hangan, R.L. Stan, **A. Turza**, L.S. Oprean, E. Pall, S. Gheorghe-Cetean, B. Sevastre, *Transit. Met. Chem.* 42, 2017, 153-164.
- [56] A.C. Hangan, **A. Turza**, R.L. Stan, L.S. Oprean. *Rev. Chim.* 69, 2019, 1407-1410.